発表者氏名	論文タイトル名	発表誌名	巻号	ページ	出版年
Miyake N, Elciog lu NH, Iida A,oth ers and Matsumot o N	PAPSS2 mutations caus e autosomal recessive b rachyolmia.	J Med Genet.	49	533-538	2012
Miyatake S, Touh o H, Miyake N, others and Matsu moto N	Sibling cases of moyam oya disease having hom ozygous and heterozygo us c.14576G>A variant in RNF213 showed var ying clinical course and severity.	J Hum Genet	57	804-806	2012
Miyatake S, Miya ke N, Doi H, Sai tsu H, Ogata K, Kawai M, Matsu moto N.	A novel SACS mutatio n in an atypical case w ith autosomal recessive spastic ataxia of Charle voix-Saguenay (ARSAC S).	Intern Med	51	2221-2226	2012
Tsurusaki Y, Sait oh S, others, Miy ake N, Matsumot o N.	A DYNC1H1 mutation causes a dominant spin al muscular atrophy wit h lower extremity predo minance.	Neurogenetics.	13	327-332	2012
Saitsu H, Kato M, others, Miyake N, Hayasaka K, Matsumoto N.	CASK aberrations in m ale patients with Ohtah ara syndrome and cereb ellar hypoplasia.	Epilepsia.	53	1441-1449	2012
Saitsu H, Kato M, others, Miyake N, Hayasaka K, Matsumoto N.	Whole exome sequencin g identifies KCNQ2 mu tations in Ohtahara syn drome.	Ann Neurol.	72	298-300	2012
Tsurusaki Y, Kos ho T, others, Miy ake N, Matsumot o N.	Exome sequencing in a family with an X-linke d lethal malformation s yndrome: clinical conse quences of hemizygous truncating OFD1 mutati ons in male patients.	Clin Genet.	83	135-144	2013
Miyatake S, Miya ke N, others, Mat sumoto N.	Homozygous c.14576G> A variant of RNF213 p redicts early-onset and severe form of moyamo ya disease.	Neurology.	78	803-810	2012
Yoneda Y, others, Miyake N, Ogata K, Naritomi K, Matsumoto N.	Missense mutations in t he DNA-binding/dimeriz ation domain of NFIX cause Sotos-like feature s.	J Hum Gene t.	57	207-11	2012

発表者氏名	論文タイトル名	発表誌名	巻号	ページ	出版年
Kondo Y, Saitsu H, others, Miyake N, Ryoo NK, Kim JH, Yu YS, Matsumoto N.	A family of oculofaciocardiodental syndrome (OFCD) with a novel BCOR mutation and genomic rearrangements involving NHS.	J Hum Genet.	57	197-201.	2012
Saitsu H, Kato M, others, Miyake N, Hayasaka K, Matsumoto N.	Association of genomic deletions in the STXBP1 gene with Ohtahara syndrome.	Clin Genet.	81	399-402	2012
Yoneda Y, Haginoya K, others, Miyake N, Yokochi K, Osaka H, Kato M, Matsumoto N, Saitsu H.	De novo and inherited mutations in COL4A2, encoding the type IV collagen α2 chain cause porencephaly.	Am J Hum Genet.	90	86-90	2012
Saitsu H, Osaka H,others, Miyake N, Harada N, Kato M, Matsumoto N.	Early infantile epileptic encephalopathy associated with the disrupted gene encoding Slit-Robo Rho GTPase activating protein 2 (SRGAP2).	Am J Med Genet A.	158A	199-205	2012

IV.　研究成果の刊行物・別刷

RESEARCH ARTICLE

Human Mutation

OFFICIAL JOURNAL

HGVS HUMAN GENOME VARIATION SOCIETY

www.hgvs.org

Mitochondrial Complex III Deficiency Caused by a Homozygous *UQCRC2* Mutation Presenting with Neonatal-Onset Recurrent Metabolic Decompensation

Noriko Miyake,[1]*† Shoji Yano,[2]† Chika Sakai,[3] Hideyuki Hatakeyama,[3] Yuichi Matsushima,[3] Masaaki Shiina,[4] Yoriko Watanabe,[5] James Bartley,[6] Jose E. Abdenur,[7] Raymond Y. Wang,[7] Richard Chang,[7] Yoshinori Tsurusaki,[1] Hiroshi Doi,[1] Mitsuko Nakashima,[1] Hirotomo Saitsu,[1] Kazuhiro Ogata,[4] Yu-ichi Goto,[3] and Naomichi Matsumoto[1]*

[1]*Department of Human Genetics, Yokohama City University Graduate School of Medicine, Yokohama, Japan;* [2]*Genetics Division, Department of Pediatrics, LAC+ USC Medical Center, Keck School of Medicine, University of Southern California, Los Angeles, California;* [3]*Department of Mental Retardation and Birth Defect Research, National Institute of Neuroscience, NCNP, Kodaira, Tokyo, Japan;* [4]*Department of Biochemistry, Yokohama City University Graduate School of Medicine, Yokohama, Japan;* [5]*Department of Pediatrics and Child Health, Kurume University School of Medicine, Kurume, Japan;* [6]*Division of Medical Genetics, Department of Pediatrics, Children's Hospital Los Angeles, Los Angeles, California;* [7]*Division of Metabolic Disorders, CHOC Children's, Orange, California*

Communicated by Daniel Nebert

Received 26 June 2012; accepted revised manuscript 7 November 2012.

Published online 19 December 2012 in Wiley Online Library (www.wiley.com/humanmutation). DOI: 10.1002/humu.22257

ABSTRACT: Mitochondrial complex III (CIII) deficiency is a relatively rare disease with high clinical and genetic heterogeneity. CIII comprises 11 subunits encoded by one mitochondrial and 10 nuclear genes. Abnormalities of the nuclear genes such as *BCS1L* and *TTC19* encoding mitochondrial assembly factors are well known, but an explanation of the majority of CIII deficiency remains elusive. Here, we report three patients from a consanguineous Mexican family presenting with neonatal onset of hypoglycemia, lactic acidosis, ketosis, and hyperammonemia. We found a homozygous missense mutation in *UQCRC2* that encodes mitochondrial ubiquinol–cytochrome *c* reductase core protein II by whole-exome sequencing combined with linkage analysis. On the basis of structural modeling, the mutation (p.Arg183Trp) was predicted to destabilize the hydrophobic core at the subunit interface of the core protein II homodimer. In vitro studies using fibroblasts from the index patient clearly indicated CIII deficiency, as well as impaired assembly of the supercomplex formed from complexes I, III, and IV. This is the first described human disease caused by a core protein abnormality in mitochondrial CIII.

Hum Mutat 00:1–10, 2012. © 2012 Wiley Periodicals, Inc.

KEY WORDS: mitochondrial complex III (CIII); *UQCRC2*; whole exome sequence; supercomplex

Introduction

The mitochondrial respiratory chain generates energy as ATP by means of the electron-transport chain and the oxidative-phosphorylation system. The mitochondrial respiratory chain, located in the inner mitochondrial membrane, is composed of five multimeric protein complexes: I, II, III, IV, and V. Among them, the complex III (CIII) (bc1 complex or ubiquinol–cytochrome *c* reductase; EC1.10.2.2) monomer is composed of 11 proteins [Iwata et al., 1998]. One protein is encoded by mitochondrial DNA (*MTCYB*) and the other 10 are encoded by nuclear DNA. The latter are categorized into three groups: (1) core proteins (encoded by *UQCRC1* and *UQCRC2*), (2) respiratory proteins (*CYC1* and *UQCRFS1*), and (3) low-molecular-weight proteins (*UQCRH*, *UQCRB*, *UQCRQ*, *UCRC*, *UQCR11*, and *UQCRFS1*). In its native state, the CIII monomer is quickly converted into a catalytically active homodimer that is incorporated into a supercomplex (respirasome) with complexes I and IV, and this supercomplex functions as a single enzyme [Schagger and Pfeiffer, 2000].

Mitochondrial CIII enzyme deficiency (CIII deficiency; MIM# 124000) is a relatively rare disease with clinical and genetic heterogeneity. Until now, mutations in four genes have been known to cause autosomal recessive CIII deficiencies: *UQCRB* (NM_006294), *UQCRQ* (NM_014402), *BCS1L* (NM_004328), and *TTC19* (NM_017775). *UQCRB* and *UQCRQ* encode components of CIII itself, whereas *BCS1L* and *TTC19* produce mitochondrial assembly factors. Although recessive *BCS1L* mutations are the most frequent cause of CIII deficiency, the majority of the genetic causes of CIII deficiency remain unknown [Benit et al., 2009; de Lonlay et al.,

Additional Supporting Information may be found in the online version of this article.

†These authors contributed equally to this work.

*Correspondence to: Noriko Miyake, Department of Human Genetics, Yokohama City University Graduate School of Medicine, 3-9 Fukuura, Kanazawa-ku, Yokohama 236-0004, Japan. E-mail: Noriko Miyake: nmiyake@yokohama-cu.ac.jp; or Naomichi Matsumoto, Department of Human Genetics, Yokohama City University Graduate School of Medicine, 3-9 Fukuura, Kanazawa-ku, Yokohama 236-0004, Japan. E-mail: naomat@yokohama-cu.ac.jp

Contract grant sponsors: Ministry of Health, Labor, and Welfare; the Japan Science and Technology Agency; the Strategic Research Program for Brain Sciences; Ministry of Education, Culture, Sports, Science, and Technology of Japan; the Japan Society for the Promotion of Science; 2011 Strategic Research Promotion of Yokohama City University; the Japan Epilepsy Research Foundation; and the Takeda Science Foundation.

2001; DiMauro and Schon, 2003; Fernandez-Vizarra et al., 2007; Hinson et al., 2007; Visapaa et al., 2002]. Interestingly, *BCS1L* mutations cause variable clinical presentations: Bjornstad syndrome (MIM# 262000), which is characterized by sensorineural hearing loss and pili torti [Hinson et al., 2007]; GRACILE syndrome (MIM# 603358), which presents with fetal growth retardation, aminoaciduria, cholestasis, iron overload, lactic acidosis, and early death [Visapaa et al., 2002]; and Leigh syndrome (MIM# 256000) [de Lonlay et al., 2001]. A homozygous mutation of *TTC19* causes a progressive neurodegenerative disorder [Ghezzi et al., 2011]. A homozygous 4-bp deletion of *UQCRB* causes hypoglycemia and lactic acidosis [Haut et al., 2003] and a homozygous missense mutation of *UQCRQ* results in severe psychomotor retardation, extrapyramidal signs, and dementia [Barel et al., 2008].

Here, we describe the first human mutation of *UQCRC2* encoding core protein 2 of CIII, utilizing linkage analysis and whole-exome sequencing.

Materials and Methods

DNA Preparation

DNAs from family members and fibroblasts from patients were collected after obtaining informed consent. DNA was extracted from blood leukocytes using a QIAamp DNA Blood Midi Kit (Qiagen, Hilden, Germany) or QuickGene-610L (Fujifilm, Tokyo, Japan), according to the manufacturers' instructions. DNAs from 80 Mexican control subjects were purchased from the Coriell Institute for Medical Research (Camden, New Jersey). The experimental protocols were approved by the institutional review board of Yokohama City University.

Linkage Analysis

SNP typing was performed using an Affymetrix Human Mapping SNP 10K Xba I 142 2.0 array (Affymetrix, Santa Clara, California), according to the manufacturer's instructions. A multipoint linkage analysis was performed using Allegro version 2.0 [Gudbjartsson et al., 2005]. An autosomal recessive mode of inheritance with complete penetrance and a disease allele frequency of 0.005 was used.

Exome Sequence

Briefly, 3 μg of genomic DNA was sheared and captured using a NimbleGen SeqCap EZ Exome Library SR (Roche NimbleGen, Inc., Madison, New Jersey), according to the manufacturer's instructions. The captured sample was sequenced on a GAIIx instrument (Illumina, Inc., San Diego, California) using 76-bp paired-end reads. Image analysis and base calling were performed by sequence-control software real-time analysis (Illumina, Inc.) and CASAVA software v1.7 (Illumina, Inc.). The quality-controlled (path-filtered) reads were mapped to human genome reference hg19 with Mapping and Assembly with Qualities (MAQ; http://maq.sourceforge.net/) and NextGENe software v2.00 (SoftGenetics, State College, Pennsylvania). The variants from MAQ were annotated by SeattleSeq annotation 131 (http://snp.gs.washington.edu/SeattleSeqAnnotation131). The priority scheme of the variants was described previously [Tsurusaki et al., 2011]. The nucleotide numbering of the variants reflects the cDNA numbering, with +1 corresponding to the A of the ATG translation initiation codon in the reference sequence, according to journal guidelines (www.hgvs.org/mutnomen). The initiation codon is codon 1.

Expression Vector Preparation

For construction of a mammalian expression vector, full-length *UQCRC2* (NM_003366.2) was amplified from a cDNA library from a multiple-tissue cDNA (MTC) panel (Clontech, Mountain View, California) using KOD-plus DNA polymerase (Toyobo, Osaka, Japan). The PCR product was cloned into the entry vector (pDONR^{TM}221) of the gateway system (Invitrogen, Carlsbad, California). Each of the two missense mutations was independently introduced into the entry clone using a QuickChange II XL site-directed mutagenesis kit (Stratagene, La Jolla, California). Each insert was cloned into pcDNA-DEST40 (C-terminal V5 and 6xHis tag) by LR recombination. All the clones were verified by direct sequencing. In addition, full-length *UQCRC2* (wild type, mutant, or SNP [rs4850: c.548G>A, p.Arg183Gln]) and AcGFP constructs were cloned into multiple cloning sites A and B of the pIRES vector (Clontech).

Intracellular Localization

Each mammalian expression construct (200 ng) was transfected into COS-1 cells using FuGENE6 (Roche Diagnostics, Indianapolis, Indiana). After 24 hr of transfection, MitoTracker Red CMXRos (Invitrogen) was added and incubated for 30 min. The cells were then fixed with 4% paraformaldehyde for 20 min at room temperature. After permeabilization with 0.1% Triton/1× PBS for 10 min, C-terminally V5-6xHis-tagged UQCRC2 protein was stained with a mouse anti-V5 antibody (1:1,000) (Invitrogen) and an Alexa Fluor 488-conjugated goat antimouse IgG secondary antibody (1:1,000) (Molecular Probes, Carlsbad, California). Confocal images were taken with a FLUOVIEW FV1000-D microscope (Olympus, Tokyo, Japan).

Mitochondrial Enzyme Activity Assay

Mitochondrial enzyme activities were measured using a previously reported method [Trounce et al., 1996], with slight modifications. The complex I activity is indicated as the rotenone-sensitive NADH–CoQ1 reductase activity. In control assays, the activity was decreased to 20% by rotenone.

Western Blotting

Mitochondrial enzyme activity and supercomplex formation were analyzed by western blotting. The enzyme activities of the mitochondrial respiratory chain complexes were measured using mitochondrial fractions prepared from primary fibroblasts derived from patient 1 ($n = 3$) and control subjects ($n = 10$). Each measurement was basically performed in triplicate (if the available materials allowed). The values were normalized to complex II or citrate synthase. Immunoblot detection of each respiratory chain complex was performed using mitochondria solubilized with 0.5% *n*-dodecyl-β-D-maltoside (DDM). The same amount of pooled mitochondrial protein from control subjects ($n = 10$) was used as the control. The primary antibodies used were as follows: 2 μg/ml anti-NDUFA9 (complex I; Invitrogen), 0.02 μg/ml anti-SDHA (complex II; Invitrogen), 2 μg/ml anti-UQCRC1 (CIII; Abcam, Cambridge, Massachusetts), 0.2 μg/ml anti-MTCO1 (complex IV; Invitrogen), and

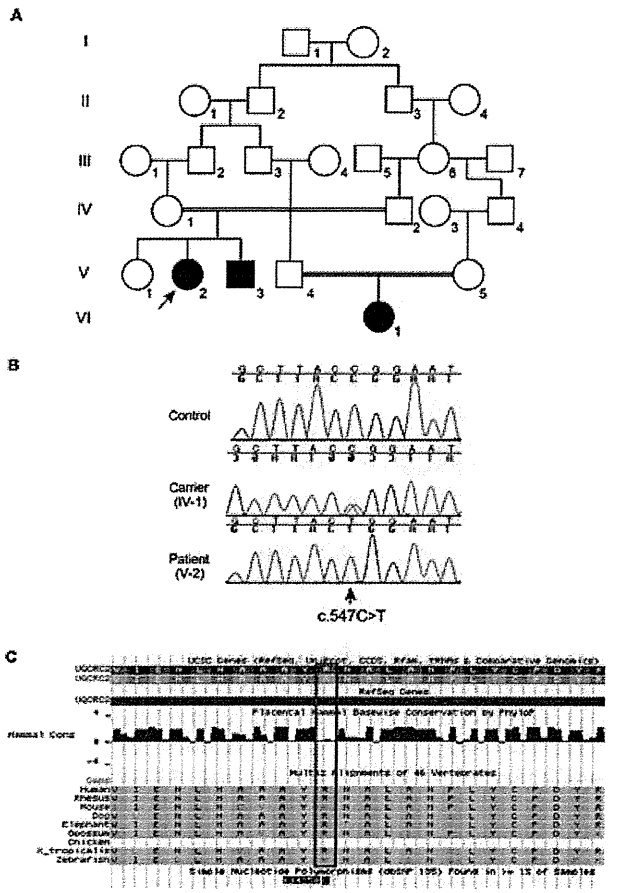

Figure 1. Identification of a *UQCRC2* mutation in a consanguineous Mexican family. **A:** Pedigree of the reported family. The arrow indicates the proband. **B:** Electropherogram of the c.547C>T *UQCRC2* mutation. All three patients (1, 2, and 3) showed a homozygous change, whereas the parents and an unaffected sibling of patients 1 and 2 were heterozygous carriers. The arrow indicates c.547C>T. **C:** Evolutionary conservation of p.Arg183 in UQCRC2 outlined in red. rs4850 (chr 16: 21976762, G>A, p.Arg183Gln) is a common SNP based on the dbSNP135 database.

2 μg/ml anti-ATP5B (complex V; Invitrogen). Immunoblot detection of the respiratory supercomplex was performed using mitochondria solubilized with 1% (w/v) digitonin. The same amount of pooled mitochondrial protein from control subjects (n = 10) was used as the control. The primary antibodies used were as follows: 0.02 μg/ml anti-SDHA (complex II; Invitrogen) and 2 μg/ml anti-UQCRC1 (CIII; Abcam). The band intensity of the supercomplex was estimated by densitometry and normalized to that of complex II. The data were obtained by three independent assays.

Results

Patient 1 (V:2 in Fig. 1A) is a Hispanic female born to a 26-year-old healthy female (G2P2Ab0) and a 28-year-old healthy male who are second cousins. She was delivered at 37 weeks by Cesarean section because of a pathological cardiotocogram. At birth, she weighed 2,329 g (5–10th percentile) with a length of 46 cm (5–10th percentile), and her occipitofrontal circumference was 34 cm (25–50th percentile). Her Apgar scores were 8, 9, and 9 at 1, 5, and 10 min, respectively. She developed a severe metabolic acidosis (pH 7.1, with a base excess of -24.6 mEq/l) within 1 day, requiring admission to a neonatal intensive care unit. Blood lactate and pyruvate on admission were 25.5 mM (reference range: <2.2 mM) and 0.436 mM (reference range: <0.16 mM), respectively (lactate to pyruvate ratio = 58.48). Clinical examination revealed tachypnea (47 breaths/min), tachycardia (181 beats/min), mild subcostal retractions, Levine II/VI systolic cardiac murmur, no organomegaly, and poor sucking reflex. Blood ammonia was 126 μM (reference range in neonates: <80 μM). The patient responded promptly to supportive therapy, with intravenous glucose infusion providing 10 mg/kg/min and a sodium bicarbonate drip improving the blood lactate level down to 12.7 mM within 24 hr. The lactate and pyruvate levels further improved to 3.1 and 0.125 mM within 3 days, respectively. Urine organic acid analysis on admission was remarkable for massive lactic and pyruvic aciduria, as well as ketonuria. Plasma amino acids were remarkable for a high alanine level (1,519 μM; reference range: 200–600 μM). Magnetic resonance imaging (MRI) of the brain revealed small right parietal and temporal infarcts.

She recovered without sequelae and was discharged on full oral feeds with a high-carbohydrate, reduced-fat formula (60% of calories from carbohydrate, 30% of calories from fat) after 1.5 months of hospitalization. She was also diagnosed with an atrial septal defect and renal tubular acidosis. After the initial hospitalization, she was hospitalized more than 10 times because of episodic metabolic decompensation with lactic acidosis (highest value was 10.8 mM at the age of 3 years and 10 months), hyperammonemia (highest value was 346 μM at the age of 3 years and 3 months), ketosis, and hypoglycemia, which were triggered by intercurrent illnesses including fevers, vomiting, and diarrhea. The patient is now 5 years of age, with normal growth and no signs of intellectual disability. The frequency of hospitalization has decreased, although she still requires urgent medical treatment with intravenous glucose infusion to prevent metabolic decompensation during intercurrent illnesses.

Patient 2 (V:3 in Fig. 1A) is a younger full sibling of patient 1. He was born at 39 weeks of gestation by repeat Cesarean section. At birth, he weighed 2,658 g (5–10th percentile) with a length of 49 cm (25–50th percentile), and his occipitofrontal circumference was 34.3 cm (25th percentile). His Apgar scores were 8 and 9 at 1 and 5 min, respectively. He developed tachypnea, grunting, and poor feeding within 1 day because of lactic acidemia. The initial capillary blood gas showed a pH of 7.05, pCO_2 of 25 mmHg, bicarbonate of 5.8 mmol/l, and a base excess of -22 mEq/l. He was intubated for 2 days and treated with intravenous glucose infusion and a bicarbonate drip to correct the metabolic acidosis. Feeding with a high-carbohydrate, reduced-fat formula was started in 10 days. His initial hospitalization was 1-month long, during which he was diagnosed with congenital lactic acidemia and persistent hypoglycemia of unknown etiology. He was treated with corticosteroid replacement therapy owing to adrenal insufficiency for 4 months until a normal adrenocorticotropic hormone stimulation test was obtained. At the age of 8 months, he was found unresponsive after 6 hr of fasting owing to decreased appetite associated with a 2-day mild upper-respiratory-tract infection. At a local emergency room, metabolic acidosis (pH 7.23), hypoglycemia (3 mg/dl; reference range: >60 mg/dl), and hyperammonemia (463 μM), as well as ketosis (blood and urine), were noted. He had five episodes of generalized seizure associated with this episode. Following treatment with levetiracetam, he has been seizure free. Brain MRI findings at the age of 8 months were unremarkable. He was hospitalized for 1 month and discharged without sequelae, and had more than 10 hospitalizations because of similar episodes of lactic acidosis, hypoglycemia, hyperammonemia, and ketosis triggered by intercurrent illnesses. Developmental delay was noted once at 4 months of age. Following

physical and speech therapy, his development was later evaluated as normal at 3 years of age. He is now 4 years of age, with normal growth and no signs of intellectual disability. Physical examination revealed neither dysmorphic features nor abnormal focal neurological signs. He has been fed with a reduced-fat, high-carbohydrate diet and fasting precautions. The frequency of hospitalization has decreased, although he continues to require urgent medical treatment with intravenous glucose infusion to prevent metabolic decompensation during intercurrent illnesses. Laboratory study data obtained in the acute severe metabolic decompensation stage at 16 months of age were remarkable, which are as follows: pH 7.19 capillary blood gas, 11 mg/dl glucose, 348 μM blood ammonia, and 6.8 mM blood lactate. Urine organic acid analysis showed markedly elevated 3-hydroxybutyrate and acetoacetate indicating severe ketosis, markedly elevated lactate and pyruvate indicating lactic acidosis, markedly elevated dicarboxylic acids (adipic acid, 1,194 mmol/mol Cr [reference range: <15 mmol/mol Cr], suberic acid, 122 mmol/mol Cr [reference range: <7 mmol/mol Cr], sebacic acid, 288 mmol/mol Cr [reference range: <2 mmol/mol Cr]) indicating hyperactive fatty acid beta oxidation, and moderately elevated tricarboxylic acid cycle intermediates including malate, fumarate, and 2-oxoglutarate. Plasma amino acids showed elevated alanine at 440 μM (reference range: 23–410 μM). Acylcarnitine profiles obtained at 19 months of age in mild decompensation showed marked elevation of C2 (48 nmol/ml [reference range: 2.6–15.5 nmol/ml]) and moderate elevation of 3-hydroxyacylcarnitines (C12–C18).

Patient 3 (VI:1 in Fig. 1A) is a girl born to consanguineous parents within the same pedigree as patients 1 and 2, but in a different branch. She was small for gestational age and was born vaginally to a 23-year-old mother after a full-term gestation. Her birth weight was 2,200 g. Initially, she had mild respiratory distress and required 1 additional day of monitoring. By 18 months of age, she had undergone four hospitalizations for vomiting, dehydration, and hypoglycemia. An initial blood examination at 18 months of age showed that her blood glucose was 17 mg/dl, bicarbonate was 8 mmol/l, and anion gap was 30 mmol/l. The simultaneous blood lactate and pyruvate levels were 26.3 mg/dl (reference range: <16.0 mg/dl) and 1.5 mg/dl (reference range: <1.5 mg/dl), respectively. She responded quickly to intravenous dextrose with correction of the hypoglycemia and metabolic acidosis. She had developmental delay and microcephaly (second percentile) that led to a brain MRI, but this was interpreted as normal. At 18 months, she spoke only two words but could follow two-part commands. She walked at 15 months of age and had low body weight until starting occupational therapy at 14 months of age. She was not dysmorphic. Her muscle strength and tone were normal when she was in good health, allowing her to climb, hop, and jump in a manner appropriate for her age.

Considering the consanguinity in this family, we hypothesized that the disease was inherited in an autosomal recessive fashion. Linkage analysis using two patients (1 and 2) and three unaffected family members (IV:1, IV:2, and V:1) indicated that homozygous regions totaling 36-Mb were shared by the two affected individuals with logarithm of the odds scores ≥2.0, as calculated by Allegro version 2 [Gudbjartsson et al., 2005] (Supp. Table S1). We then performed whole-exome sequencing of DNA from patient 1. Two homozygous variants within the 36-Mb homozygous regions were identified: c.547C>T, p.Arg183Trp in *UQCRC2* (NM_003366) and c.1675A>G, p.Met559Val in *TNRC6A* (NM_014494). Sanger sequencing confirmed the two variants in patient 1. The Polyphen-2 program (http://genetics.bwh.harvard.edu/pph2/) predicted that p.Arg183Trp in *UQCRC2* and p.Met559Val in *TNRC6A* were probably damaging and benign, respectively (Table 1). *TNRC6A* was ruled out as a candidate because the heterozygous *TNRC6A* change was found in patient 3. *UQCRC2* encodes ubiquinol–cytochrome *c* reductase core protein II (UQCRC2; MIM# 191329), a core protein of CIII. All three patients possessed the homozygous p.Arg183Trp change in *UQCRC2*, whereas the father (IV-2), mother (IV-1), and sister (V-1) (all unaffected) were heterozygous (Fig. 1B). This change was not observed among 80 Mexican control alleles or 750 Japanese control alleles.

Table 1. Prediction of Mutational Effects in UQCRC2

Mutation	Alteration	Type	Grantham score[a]	Polyphen-2	Energy ddG[b]
c.547C>T	p.Arg183Trp	Mutant	101	0.998	10.02
c.548G>A	p.Arg183Gln	SNP	43	0.177	2.19
c.547_548CG>AA	p.Arg183Lys	Ortholog	26	0.001	1.74

[a]Grantham score indicates the chemical dissimilarity caused by codon replacements.
[b]The corrected average interaction energy ddG of each altered amino acid is calculated by FoldX as homozygous mutation.

To predict the effect of the missense mutation (c.547C>T, p.Arg183Trp) on the structural stability of CIII, we calculated the free-energy change of interactions between the core protein monomers (encoded by *UQCRC2*) with and without the mutation using FoldX software (version 3.0) [Guerois et al., 2002; Khan and Vihinen, 2010]. For this calculation, we used the crystal structure of bovine CIII (PDB code 2A06) as a structural model because no crystal structure is available for human UQCRC2. Amino acid position 183 of UQCRC2 is a highly conserved basic amino acid among species from zebrafish to humans (e.g., Arg in humans and cows, Lys in mice; Fig. 1C) and is reported to be substituted for Gln as a nonsynonymous human SNP (rs4850 [c.548G>A, p.Arg183Gln]) (Fig. 1C). Therefore, we also calculated the interaction-energy change upon replacement of Arg183 with Lys or Gln, in addition to the Trp found in the patient. The calculated interaction-energy change caused by replacement of Arg183 with Trp was estimated as 10 kcal/mol, whereas those caused by replacement with Lys or Gln were no more than 2 kcal/mol (Fig. 2A, Table 1). The molecular structure of the wild-type core protein homodimer indicated that the methylene part of the Arg183 side chain of one subunit forms a hydrophobic core with the side chains of His254 and Phe449 of the other subunit at the homodimer interface (Fig. 2B and C). When the Arg183 of the core protein was replaced by Trp, the introduced Trp183 side chain flipped outward from the original side-chain position because of steric hindrance (Fig. 2D). In contrast, when Arg183 was replaced by Lys or Gln, each side chain occupied the original position to maintain a hydrophobic core with the methylene part of Lys or Gln (Fig. 2E and F). This indicates that the Arg183Trp mutation in UQCRC2 would disrupt the hydrophobic core formed at the interface of the UQCRC2-containing complex, resulting in destabilization of CIII. In vitro experiments showing that the exogenous and endogenous expressions of the UQCRC2 mutant were significantly reduced (Supp. Figs. S1 and S2) may support the protein instability.

To test whether this mutation alters UQCRC2 localization at the mitochondrial inner membrane, we created mammalian full-length wild-type, mutant, and SNP (rs4850) constructs; transiently overexpressed them in COS1 cells; and observed their localization microscopically. The mutant protein colocalized with mitochondria, similar to the wild-type and SNP proteins (Supp. Fig. S3). This indicates that the p.Arg183Trp mutation probably does not alter the intracellular localization.

To evaluate mitochondrial function in vitro, we measured the enzyme activities of the mitochondrial respiratory chain complexes

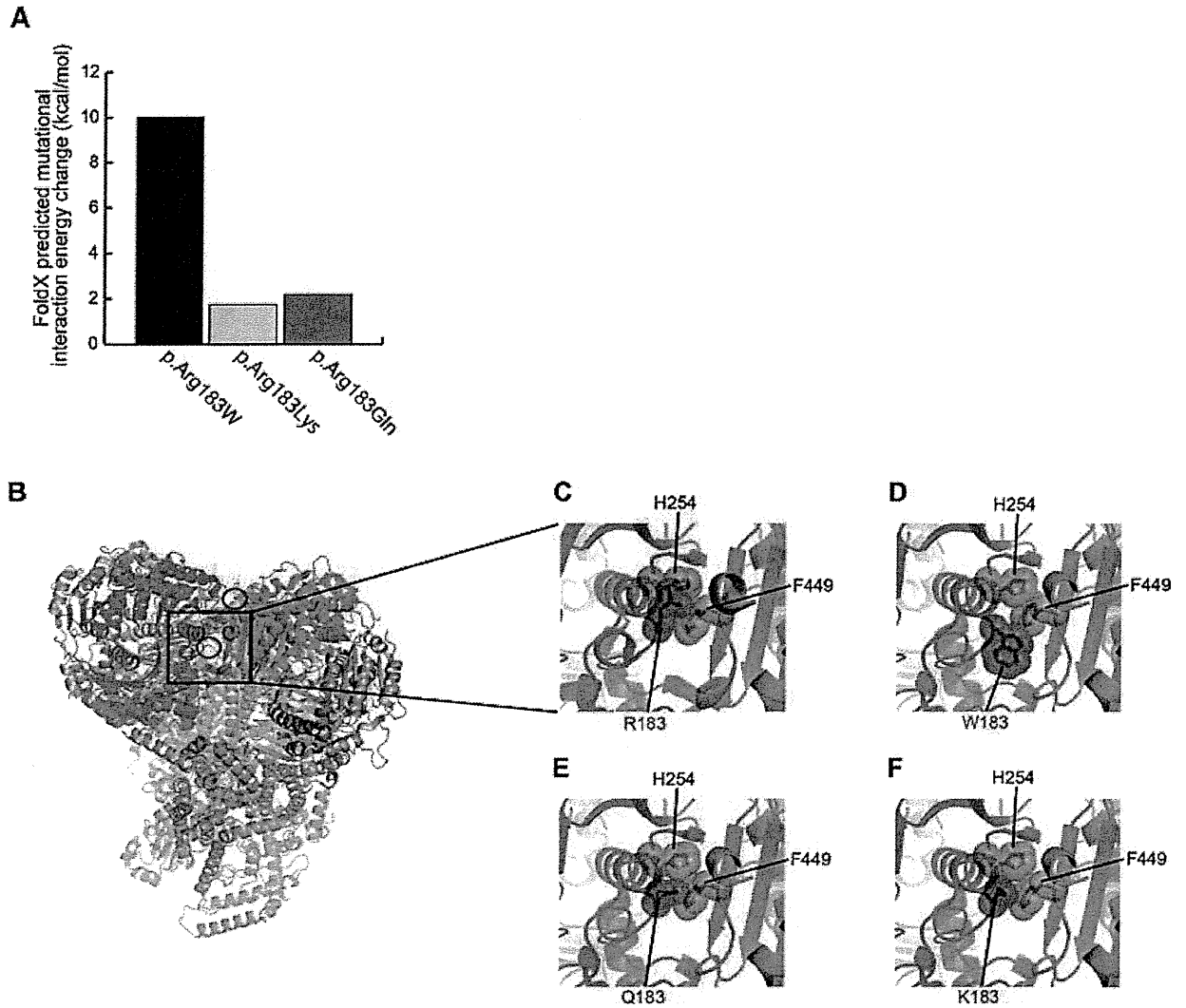

Figure 2. Molecular structural consideration of the effect on dimerization of amino acid replacement at residue position 183 in the core protein. **A:** Calculated interaction-energy change of the core protein homodimer upon replacement by the indicated amino acids at residue 183 using FoldX software. **B:** Overview of the crystal structure of the bovine mitochondrial bc1 (CIII) complex (PDB code 2A06). The core protein monomers are colored green and cyan; the other components are shown in gray. The helices, strands, and loops are shown as ribbons, arrows, and threads, respectively. The red circle indicates residue 183 in the core protein. The box corresponds to the enlarged areas shown in parts **(C)–(F). C–F:** Detailed views of the core protein homodimerization interface in the wild-type **(C)** and mutated, polymorphic, orthologous (p.Arg183Trp/Gln/Lys) **(D, E, F,** respectively) complex structures. The residues at amino acid 183 of one subunit (red), and His254 and Phe449 of the other subunit (orange) are shown as sticks with Connolly surfaces. All graphics were drawn using PyMOL (www.pymol.com).

using mitochondrial fractions prepared from primary fibroblasts derived from patient 1. With normalization to complex II activity, the CIII activity of patient 1 was decreased to 50% of that in the control subjects (n = 10), whereas complex I activity increased by threefold and complex IV activity remained at the same level as in the control subjects (Fig. 3A). Similar results were obtained using normalization to citrate synthase activity (Fig. 3B). We also investigated the steady-state level of the respiratory complexes by blue-native polyacrylamide gel electrophoresis (BN-PAGE) using the same mitochondrial fraction used for the enzyme activity measurements. For analysis of individual complexes, mitochondria were solubilized with 0.5% (w/v) DDM. For analysis of the supercomplex (complexes I, III, and IV), mitochondria were solubilized with 1% (w/v) digitonin. After BN-PAGE, we performed immunoblotting with specific antibodies for the respiratory complexes (Fig. 3C–F, Supp. Notes, and Supp. Fig. S4). In the patient's fibroblasts, we found that CIII and supercomplex assembly were decreased to 18%–20% $\gg$ 22% –23% (Fig. 3C and D) and 4% $\gg$ 7.5% (Fig. 3E and F) of the levels in pooled control samples, respectively. These data indicate that a homozygous missense mutation (c.547C>T, p.Arg183Trp) in *UQCRC2* causes moderately impaired CIII function and severely decreased amounts of CIII and supercomplex, which would be the primary molecular pathogenesis in the patients.

Discussion

Among the genes known to cause CIII deficiency, impairment of UQCRC2, as found in our patients, leads to a similar clinical course to that reported for UQCRB defects with recurrent crises of

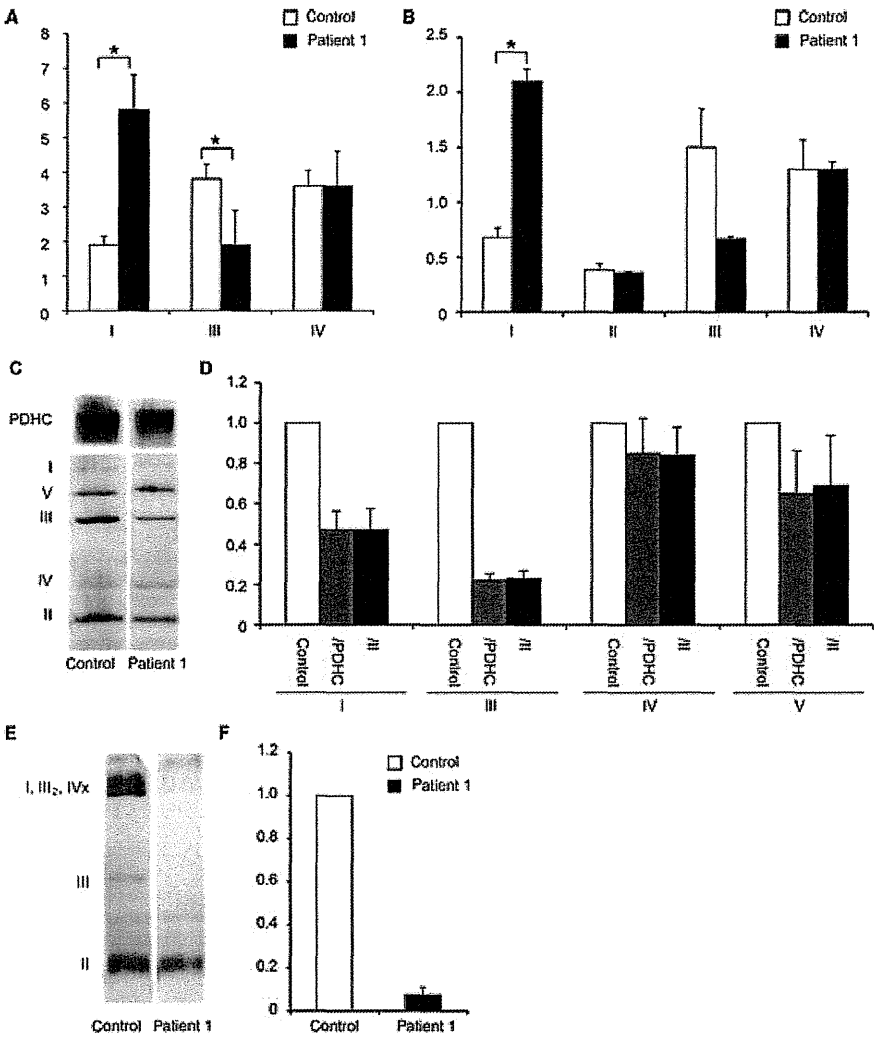

Figure 3. Mitochondrial enzyme activity and supercomplex formation. **A, B:** Enzyme activities of the mitochondrial respiratory chain complexes using mitochondrial fractions prepared from primary fibroblasts derived from patient 1 ($n = 3$) and control subjects ($n = 10$). Each measurement was performed in triplicate. The values were normalized to complex II (**A**) or citrate synthase (**B**). Error bars represent the SEM. **C, D:** Immunoblot detection of each respiratory chain complex using mitochondria solubilized with 0.5% DDM. The same amount of pooled mitochondrial protein from control subjects ($n = 10$) was loaded into the control lane. The band intensity of each respiratory complex was estimated by densitometry and normalized to that of PDHC (gray bar) or complex II (black bar). The data were obtained by three independent assays and the error bars in (**D**) represent the SEM. **E, F:** Immunoblot detection of the respiratory supercomplex using mitochondria solubilized with 1% (w/v) digitonin. The same amount of pooled mitochondrial protein from control subjects ($n = 10$) was loaded into the control lane. The band intensity of the supercomplex was estimated by densitometry and normalized to that of complex II (black bar). The data were obtained by three independent assays and the error bars in (**F**) represent the SEM.

hypoglycemia, lactic acidosis, and ketosis, although the latter did not show hyperammonemia. In contrast, impairment of BCS1L, TTC19, and UQCRQ leads to rather severe complications such as intrauterine growth retardation, liver failure, tubulopathy, sensorineural hearing loss, and abnormalities on brain MRI. The normal development in our patients, despite frequent metabolic crises, may suggest that the UQCRC2 phenotype in our family is milder than disorders of the CIII genes and that this UQCRC2 abnormality does not primarily affect the brain. However, patients 2 and 3 showed epilepsy, and developmental delay was noted in patient 3. It remains to be seen whether this clinical variability is caused by variable expressivity, unknown modifiers, or secondary to the severity of the acute metabolic crises. Interestingly, our patients showed hyperammonemia, highly abnormal urine organic acids indicative of mitochondrial dysfunction, and highly elevated plasma hydroxyl fatty acids during their crises, whereas patients with the other reported CIII impairment disorders did not [Barel et al., 2008; de Lonlay et al., 2001; Ghezzi et al., 2011; Haut et al., 2003; Hinson et al., 2007; Visapaa et al., 2002]. These observations may imply that *UQCRC2* mutations have secondary effects in other metabolic pathways including the Krebs cycle, beta oxidation, and urea cycle.

Conclusion

We have identified, for the first time, a homozygous mutation in human *UQCRC2* encoding a core protein of mitochondrial CIII. Further studies of additional patients with *UQCRC2* abnormalities are necessary to fully understand human CIII disorders.

Acknowledgments

We thank all the family members for participating in this study. We also thank the Commission for Families and Children of Orange County for its support of our clinical work. We appreciate Dr. Takeyori Saheki for useful comments on metabolic decompensation. This study was performed at the Advanced Medical Research Center, Yokohama City University.

Disclosure statement: The authors have no conflict of interest to declare.

References

Barel O, Shorer Z, Flusser H, Ofir R, Narkis G, Finer G, Shalev H, Nasasra A, Saada A, Birk OS. 2008. Mitochondrial complex III deficiency associated with a homozygous mutation in UQCRQ. Am J Hum Genet 82:1211–1216.

Benit P, Lebon S, Rustin P. 2009. Respiratory-chain diseases related to complex III deficiency. Biochim Biophys Acta 1793:181–185.

de Lonlay P, Valnot I, Barrientos A, Gorbatyuk M, Tzagoloff A, Taanman JW, Benayoun E, Chretien D, Kadhom N, Lombes A, de Baulny HO, Niaudet P, et al. 2001. A mutant mitochondrial respiratory chain assembly protein causes complex III deficiency in patients with tubulopathy, encephalopathy and liver failure. Nat Genet 29:57–60.

DiMauro S, Schon EA. 2003. Mitochondrial respiratory-chain diseases. N Engl J Med 348:2656–2668.

Fernandez-Vizarra E, Bugiani M, Goffrini P, Carrara F, Farina L, Procopio E, Donati A, Uziel G, Ferrero I, Zeviani M. 2007. Impaired complex III assembly associated with BCS*1L* gene mutations in isolated mitochondrial encephalopathy. Hum Mol Genet 16:1241–1252.

Ghezzi D, Arzuffi P, Zordan M, Da Re C, Lamperti C, Benna C, D'Adamo P, Diodato D, Costa R, Mariotti C, Uziel G, Smiderle C, et al. 2011. Mutations in TTC*19* cause mitochondrial complex III deficiency and neurological impairment in humans and flies. Nat Genet 43:259–263.

Gudbjartsson DF, Thorvaldsson T, Kong A, Gunnarsson G, Ingolfsdottir A. 2005. Allegro version 2. Nat Genet 37:1015–1016.

Guerois R, Nielsen JE, Serrano L. 2002. Predicting changes in the stability of proteins and protein complexes: a study of more than 1000 mutations. J Mol Biol 320:369–387.

Haut S, Brivet M, Touati G, Rustin P, Lebon S, Garcia-Cazorla A, Saudubray JM, Boutron A, Legrand A, Slama A. 2003. A deletion in the human QP-C gene causes a complex III deficiency resulting in hypoglycaemia and lactic acidosis. Hum Genet 113:118–122.

Hinson JT, Fantin VR, Schonberger J, Breivik N, Siem G, McDonough B, Sharma P, Keogh I, Godinho R, Santos F, Esparza A, Nicolau Y, et al. 2007. Missense mutations in the BCS*1L* gene as a cause of the Bjornstad syndrome. N Engl J Med 356:809–819.

Iwata S, Lee JW, Okada K, Lee JK, Iwata M, Rasmussen B, Link TA, Ramaswamy S, Jap BK. 1998. Complete structure of the 11-subunit bovine mitochondrial cytochrome bc1 complex. Science 281:64–71.

Khan S, Vihinen M. 2010. Performance of protein stability predictors. Hum Mutat 31:675–684.

Mitsuhashi S, Hatakeyama H, Karahashi M, Koumura T, Nonaka I, Hayashi YK, Noguchi S, Sher RB, Nakagawa Y, Manfredi G, Goto Y, Cox GA, Nishino I. 2011. Muscle choline kinase beta defect causes mitochondrial dysfunction and increased mitophagy. Hum Mol Genet 20:3841–3851.

Schagger H, Pfeiffer K. 2000. Supercomplexes in the respiratory chains of yeast and mammalian mitochondria. EMBO J 19:1777–1783.

Trounce IA, Kim YL, Jun AS, Wallace DC. 1996. Assessment of mitochondrial oxidative phosphorylation in patient muscle biopsies, lymphoblasts, and transmitochondrial cell lines. Methods Enzymol 264:484–509.

Tsurusaki Y, Osaka H, Hamanoue H, Shimbo H, Tsuji M, Doi H, Saitsu H, Matsumoto N, Miyake N. 2011. Rapid detection of a mutation causing X-linked leucoencephalopathy by exome sequencing. J Med Genet 48:606–609.

Visapaa I, Fellman V, Vesa J, Dasvarma A, Hutton JL, Kumar V, Payne GS, Makarow M, Van Coster R, Taylor RW, Turnbull DM, Suomalainen A, et al. 2002. GRACILE syndrome, a lethal metabolic disorder with iron overload, is caused by a point mutation in BCS*1L*. Am J Hum Genet 71:863–876.

BRIEF REPORT

Human Mutation

OFFICIAL JOURNAL

HGVS HUMAN GENOME VARIATION SOCIETY www.hgvs.org

KDM6A Point Mutations Cause Kabuki Syndrome

Noriko Miyake,[1]* Seiji Mizuno,[2] Nobuhiko Okamoto,[3] Hirofumi Ohashi,[4] Masaaki Shiina,[5] Kazuhiro Ogata,[5] Yoshinori Tsurusaki,[1] Mitsuko Nakashima,[1] Hirotomo Saitsu,[1] Norio Niikawa,[6] and Naomichi Matsumoto[1]

[1]Department of Human Genetics, Yokohama City University Graduate School of Medicine, Yokohama, Japan; [2]Department of Pediatrics, Central Hospital, Aichi Human Service Center, Kasugai, Japan; [3]Division of Medical Genetics, Osaka Medical Center and Research Institute for Maternal and Child Health, Izumi, Japan; [4]Division of Medical Genetics, Saitama Children's Medical Center, Iwatsuki, Japan; [5]Department of Biochemistry, Yokohama City University Graduate School of Medicine, Yokohama, Japan; [6]Research Institute of Personalized Health Sciences, Health Science University of Hokkaido, Hokkaido, Japan

Communicated by Garry R. Cutting

Received 7 August 2012; accepted revised manuscript 18 September 2012.
Published online 19 October 2012 in Wiley Online Library (www.wiley.com/humanmutation). DOI: 10.1002/humu.22229

ABSTRACT: Kabuki syndrome (KS) is a rare congenital anomaly syndrome characterized by a unique facial appearance, growth retardation, skeletal abnormalities, and intellectual disability. In 2010, *MLL2* was identified as a causative gene. On the basis of published reports, 55–80% of KS cases can be explained by *MLL2* abnormalities. Recently, de novo deletion of *KDM6A* has been reported in three KS patients, but point mutations of *KDM6A* have never been found. In this study, we investigated *KDM6A* in 32 KS patients without an *MLL2* mutation. We identified two nonsense mutations and one 3-bp deletion of *KDM6A* in three KS cases. This is the first report of *KDM6A* point mutations associated with KS.
Hum Mutat 34:108–110, 2013. © 2012 Wiley Periodicals, Inc.

KEY WORDS: Kabuki syndrome; *KDM6A*; point mutations; chromosome X

Kabuki syndrome (KS; MIM# 147920), first described by Niikawa and Kuroki in 1981, is a rare congenital anomaly syndrome with the characteristic facial features of a long palpebral fissure and eversion of lateral third of the inferior eyelids [Kuroki et al., 1981; Niikawa et al., 1981]. Individuals with KS also show mild to severe intellectual disability, growth retardation, skeletal abnormalities, and a variety of visceral malformations. Although KS is thought to inherit in autosomal dominant fashion, other inheritance patterns have also been considered [Matsumoto and Niikawa, 2003]. In 2010, whole exome sequencing successfully identified loss-of-function mutations in *MLL2* in KS. *MLL2* maps to 12q13.12 and consists of at least 54 coding exons. *MLL2* encodes a histone H3 lysine 4 (H3K4)-specific methyl transferase and plays important roles in the epigenetic control of active chromatin states. On the basis of recent reports of *MLL2* mutations in KS, the mutation detection rate of *MLL2* in KS is 55–80% [Banka et al., 2012]. Among the published mutations, 73.2% (170/232) were truncation type, and pathogenic missense mutations were mainly localized in exon 48 [Banka et al., 2012].

X-linked inheritance has also been implicated in KS. Sex chromosome abnormalities in KS have been reported many times and some of the clinical manifestations are shared with Turner syndrome; patients showing overlapping features, called "Turner–Kabuki" syndrome, have been reported [Bianca et al., 2009; Dennis et al., 1993; Niikawa et al., 1988; Rodriguez et al., 2008; Stankiewicz et al., 2001; Wellesley and Slaney, 1994]. Common structural abnormalities (inversion, translocation, and ring chromosome) involving Xp11 and Yp11 in the pseudoautosomal region were observed in KS, implying the potential involvement of the regions for pathogenesis in KS [Matsumoto and Niikawa, 2003]. In addition, two unrelated KS patients with ring X (p11.2q13) have been reported [McGinniss et al., 1997; Niikawa et al., 1988]. However, an X-linked gene for KS has not been identified until recently. In 2012, complete or partial de novo deletions of *KDM6A* (MIM# 300228) were identified in three patients with KS [Lederer et al., 2012]. *KDM6A* resides at Xp11.3 and encodes the lysine demethylase 6A (KDM6A) demethylating di- and trimethyl-lysine 27 on histone H3 (H3K27) [Lee et al., 2007]. H3K4 methylation by MLL2/3 is linked to the demethylation of H3K27 by KDM6A [Lee et al., 2007]. These authors sequenced *KDM6A* in their series of 22 patients, but found no point mutations [Lederer et al., 2012]. In this study, we investigated *KDM6A* with regard to point mutations in KS after obtaining written informed consents from families of patients. The institutional review board of Yokohama City University School of Medicine approved this study.

To identify *KDM6A* mutations in KS, we examined this gene's 29 coding exons along with its exon–intron boundaries (NM_021140.2) in 32 KS individuals with no *MLL2* mutation, using high-resolution melting analysis combined with direct sequencing. We identified three mutations: c.3717G>A (p.Trp1239*) in patient 1 (male, hemizygous), c.1555C>T (p.Arg519*) in patient 2 (male, hemizygous), and c.3354_3356delTCT (p.Leu1119del) in patient 3 (female, heterozygous) (Fig. 1). Nucleotide numbering reflects cDNA numbering with +1 corresponding to the A of the ATG translation initiation codon in the reference sequence (NM_021140.2), according to journal guidelines (www.hgvs.org/mutnomen). The initiation codon is codon 1. One mutation (c.3354_3356delTCT) occurred de novo; parental samples were unavailable for the other two. Because the two nonsense mutations were outside of the last

Additional Supporting Information may be found in the online version of this article.

*Correspondence to: Noriko Miyake, Department of Human Genetics, Yokohama City University Graduate School of Medicine, 3-9 Fukuura, Kanazawa-ku, Yokohama 236-0004, Japan. E-mail: nmiyake@yokohama-cu.ac.jp or Naomichi Matsumoto, E-mail: naomat@yokohama-cu.ac.jp

Contract grant sponsors: Ministry of Health, Labour, and Welfare (Japan) (to N.Mi., H.S., and N.Ma.); Japan Science and Technology Agency (to N.Ma.); Strategic Research Program for Brain Sciences from the Ministry of Education, Culture, Sports, Science, and Technology of Japan (to N.Ma.); Japan Society for the Promotion of Science (to N.Mi., H.S., and N.Ma.); Strategic Research Promotion of Yokohama City University (to N.Ma.); Takeda Science Foundation (to N.Mi. and N.Ma.).

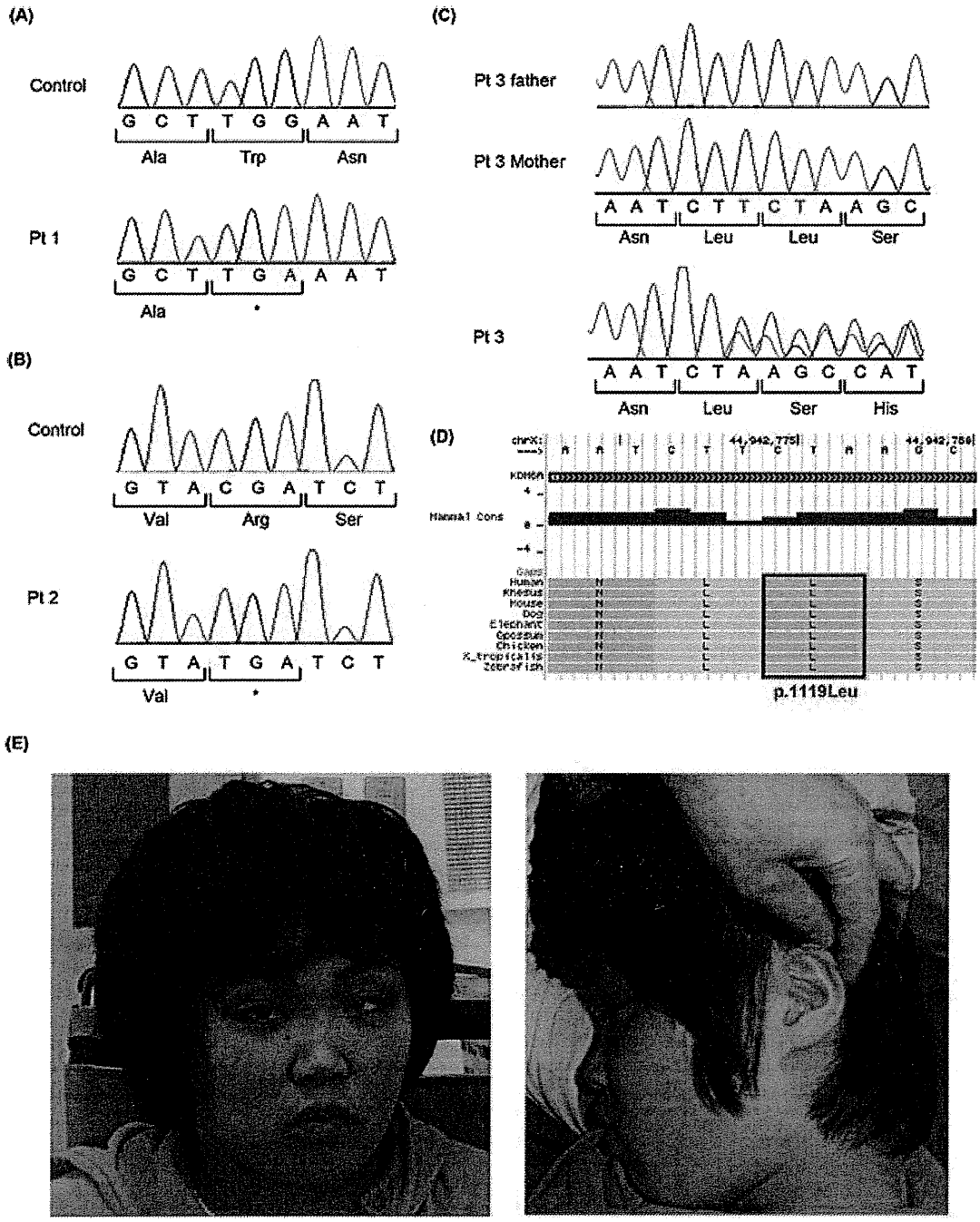

Figure 1. *KDM6A* mutations in three Kabuki syndrome patients. **A–C:** Electropherogram of patient 1: c.3717G>A (p.Trp1239*) (**A**), patient 2: c.1555C>T (p.Arg519*) (**B**), and patient 3: c.3354_3356delTCT (p.Leu1119del) (**C**). Hemizygous changes (**A** and **B**) and a heterozygous change (**C**) can be seen. The altered or deleted nucleotides are written in red. **D:** p. Leu1119 is evolutionarily conserved from zebrafish to human. The position of p.Leu1119 is boxed in red. **E:** Facial photographs of patient 3.

coding exon, and in an exon 55 bp from the 3′ most exon–exon junction, the mutant alleles could be subjected to nonsense-mediated mRNA decay (unfortunately living cells from the patients were unavailable, so we could not test this hypothesis). c.3354_3356delTCT in patient 3 would lead to deletion of one amino acid within the functionally important catalytic Jumonji C (JmjC) domain [Lee et al., 2007]. The amino residue p.Leu1119 is evolutionarily conserved from zebrafish to human (Fig. 1D) and plays an important role in hydrophobic core formation with p.Ile1126 and p.Met1129 to stabilize the JmjC domain [Sengoku and Yokoyama, 2011]. This amino acid deletion may impair helix formation around the mutated residue, resulting in domain destabilization.

Basically, *KDM6A*/*Kdm6a* escapes X-inactivation in humans and mice [Greenfield et al., 1998; Xu et al., 2008]. However, its expression from the inactive X chromosome is lower (15–35%) than that from the active X chromosome in female mice; thus, *Kdm6a* expression

Table 1. Clinical Features of Patients with a *KDM6A* Mutation

	Patient 1	Patient 2	Patient 3
Sex	Male	Male	Female
Mutation	c.3717G>A	c.1555C>T	c.3354_3356delTCT
Protein change	p.Trp1239*	p.Arg519*	p.Leu1119del
De novo status	NA	NA	De novo
Paternal age at birth	34	42	27
Maternal age at birth	33	40	26
Characteristic face	+	+	+
Microcephaly	+	+	–
Long palpebral fissures	+	+	+
Epicanthus	+	–	–
Lower palpebral eversion	+	+	+
Prominent ear	+	+	–
Auricular deformity	+	+	–
Depressed nasal tip	+	+	NA
Short nasal septum	+	+	NA
Abnormal dentition	+	+	–
Hypodontia	+	+	–
High-arched palate	+	+	–
Micrognathia	+	–	–
Short fifth finger	+	–	+
Developmental delay	+ (Severe)	+ (Severe)	+ (Severe)
Intellectual disability	+ (Severe)	+ (Severe)	+ (Severe)
Short stature	+	+	+
Prenatal growth retardation	+ (–1.96 SD)	+	–
Postnatal growth retardation	+	+	+
Cardiovascular abnormality	+	–	–
Joint laxity	+	+	–
Recurrent otitis media	+	–	–
Deafness	+[a]	–	NA
Karyotype	46,XY	46,XY	46,XX

[a]The deafness in patient 1 is conductive because of recurrent otitis media.
KDM6A gene variants were deposited in a gene-specific database (http://www.lovd.Nl/KDM6A).
NA, not analyzed.

in female mice was not twice that in male mice [Xu et al., 2008]. In addition, *UTY* (Yq11.221), a paralog of *KDM6*, has been suspected to partially compensate in males while its function is not well known [Lederer et al., 2012; Xu et al., 2008]. Patient 3 in our study showed a random pattern of X-inactivation with the ratio 57:43 in genomic DNA of peripheral leukocytes. Interestingly, marked skewing of X-inactivation was observed in two female patients reported by Lederer et al. (2012). In their lymphoblast, *KDM6A* deletion was recognized at inactive X chromosome in all 70 mitoses. Here, we propose the threshold model for the pathogenicity of *KDM6A* abnormality (Supp. Fig. S1). The two female patients with a *KDM6A* deletion might not attain the appropriate level of *KDM6A* expression allowing normal development due to existence of specific cells with unfavorable inactivation, whereas male and pure Turner syndrome female with appropriate *KDM6A* expression do not show KS phenotype under assumption of unknown partial functional compensation of *KDM6A* by *UTY* in Y chromosome (only for male) (Supp. Fig. S1).

We reviewed the clinical details of the three patients (Table 1; Supp. Text). All patients were born to unrelated healthy parents. All the three showed severe developmental delay and intellectual disability. Interestingly, patient 3 (female) presented less dysmorphic features and the two male patients 1 and 2 showed a much more severe phenotype with multiple organ involvement (Table 1; Fig. 1E). Null expression of *KDM6A* in males and residual *KDM6A* expression from active X chromosome may explain sex-biased severity (Supp. Fig. S1). Alternatively, it could be explained by a lesser effect of the in-frame mutation in female patient. However, in a previous study, the severity of clinical symptoms varied also among two female patients and a male with a *KDM6A* deletion [Lederer et al., 2012]. More studies of KS patients with *KDM6A* abnormality are necessary. It is likely that the mutation type as well as the X-inactivation pattern in affected organs in females may determine the severity of KS.

In conclusion, we have described the first three point mutations of *KDM6A* in KS. Our three patients out of 32 *MLL2*-negative patients (mutation detection rate: 9.3%) are comparable to the three patients out of 22 *MLL2*-negative patients (13.6%) previously described [Lederer et al., 2012], regardless of the mutation type. The mutation detection rates for *MLL2* (55–80%) plus *KDM6A* (9–13%) in KS suggest that other gene(s) may be found. Because both MLL2 and KDM6A are histone modifiers, the other pathogenic genes might have related functions. Further research is needed to understand the pathomechanisms of KS as well as the role of histone modification in human disease.

Acknowledgments

We thank the patients and their families for participating in this work. We also thank Ms. Y. Yamashita and Ms. S. Sugimoto for technical assistance.

References

Banka S, Veeramachaneni R, Reardon W, Howard E, Bunstone S, Ragge N, Parker MJ, Crow YJ, Kerr B, Kingston H, Metcalfe K, Chandler K, et al. 2012. How genetically heterogeneous is Kabuki syndrome? MLL2 testing in 116 patients, review and analyses of mutation and phenotypic spectrum. Eur J Hum Genet 20:381–388.

Bianca S, Barrano B, Cataliotti A, Indaco L, Ingegnosi C, Ettore G. 2009. Kabuki syndrome and sex chromosomal anomalies: is it really an association? Fertil Steril 91:e6.

Dennis NR, Collins AL, Crolla JA, Cockwell AE, Fisher AM, Jacobs PA. 1993. Three patients with ring (X) chromosomes and a severe phenotype. J Med Genet 30:482–486.

Greenfield A, Carrel L, Pennisi D, Philippe C, Quaderi N, Siggers P, Steiner K, Tam PP, Monaco AP, Willard HF, Koopman P. 1998. The UTX gene escapes X inactivation in mice and humans. Hum Mol Genet 7:737–742.

Kuroki Y, Suzuki Y, Chyo H, Hata A, Matsui I. 1981. A new malformation syndrome of long palpebral fissures, large ears, depressed nasal tip, and skeletal anomalies associated with postnatal dwarfism and mental retardation. J Pediatr 99:570–573.

Lederer D, Grisart B, Digilio MC, Benoit V, Crespin M, Ghariani SC, Maystadt I, Dallapiccola B, Verellen-Dumoulin C. 2012. Deletion of KDM6A, a histone demethylase interacting with MLL2, in three patients with Kabuki syndrome. Am J Hum Genet 90:119–124.

Lee MG, Villa R, Trojer P, Norman J, Yan KP, Reinberg D, Di Croce L, Shiekhattar R. 2007. Demethylation of H3K27 regulates polycomb recruitment and H2A ubiquitination. Science 318:447–450.

Matsumoto N, Niikawa N. 2003. Kabuki make-up syndrome: a review. Am J Med Genet 117C:57–65.

McGinniss MJ, Brown DH, Burke LW, Mascarello JT, Jones MC. 1997. Ring chromosome X in a child with manifestations of Kabuki syndrome. Am J Med Genet 70:37–42.

Niikawa N, Kuroki Y, Kajii T, Matsuura N, Ishikiriyama S, Tonoki H, Ishikawa N, Yamada Y, Fujita M, Umemoto H, Iwama Y, Kondoh I, et al. 1988. Kabuki make-up (Niikawa–Kuroki) syndrome: a study of 62 patients. Am J Med Genet 31:565–589.

Niikawa N, Matsuura N, Fukushima Y, Ohsawa T, Kajii T. 1981. Kabuki make-up syndrome: a syndrome of mental retardation, unusual facies, large and protruding ears, and postnatal growth deficiency. J Pediatr 99:565–569.

Rodriguez L, Diego-Alvarez D, Lorda-Sanchez I, Gallardo FL, Martinez-Fernandez ML, Arroyo-Munoz ME, Martinez-Frias ML. 2008. A small and active ring X chromosome in a female with features of Kabuki syndrome. Am J Med Genet 146A:2816–21.

Sengoku T, Yokoyama S. 2011. Structural basis for histone H3 Lys 27 demethylation by UTX/KDM6A. Genes Dev 25:2266–2277.

Stankiewicz P, Thiele H, Giannakudis I, Schlicker M, Baldermann C, Kruger A, Dorr S, Starke H, Hansmann I. 2001. Kabuki syndrome-like features associated with a small ring chromosome X and XIST gene expression. Am J Med Genet 102:286–292.

Wellesley DG, Slaney S. 1994. Kabuki make-up and Turner syndromes in the same patient. Clin Dysmorphol 3:297–300.

Xu J, Deng X, Watkins R, Disteche CM. 2008. Sex-specific differences in expression of histone demethylases Utx and Uty in mouse brain and neurons. J Neurosci 28:4521–4527.

Journal of Human Genetics (2012), 1–3

www.nature.com/jhg

SHORT COMMUNICATION

The diagnostic utility of exome sequencing in Joubert syndrome and related disorders

Yoshinori Tsurusaki[1], Yasuko Kobayashi[2], Masataka Hisano[3], Shuichi Ito[4], Hiroshi Doi[1], Mitsuko Nakashima[1], Hirotomo Saitsu[1], Naomichi Matsumoto[1] and Noriko Miyake[1]

Joubert syndrome (JS) and related disorders (JSRD) are autosomal recessive and X-linked disorders characterized by hypoplasia of the cerebellar vermis with a characteristic 'molar tooth sign' on brain imaging and accompanying neurological symptoms including episodic hyperpnoea, abnormal eye movements, ataxia and intellectual disability. JSRD are clinically and genetically heterogeneous, and, to date, a total of 17 causative genes are known. We applied whole-exome sequencing (WES) to five JSRD families and found mutations in all: either *CEP290*, *TMEM67* or *INPP5E* was mutated. Compared with conventional Sanger sequencing, WES appears to be advantageous with regard to speed and cost, supporting its potential utility in molecular diagnosis.
Journal of Human Genetics advance online publication, 4 October 2012; doi:10.1038/jhg.2012.117

Keywords: *CEP290*; exome sequencing; *INPP5E*; Joubert syndrome; molecular diagnosis; *TMEM67*

Joubert syndrome (JS) and related disorders (JSRD) are autosomal recessive and X-linked disorders characterized by hypoplasia of the cerebellar vermis with the characteristic neuroradiological 'molar tooth sign' and accompanying neurological symptoms including dysregulation of breathing pattern, ataxia and developmental delay. JSRD are classified into six subtypes: pure JS, JS with ocular defect, JS with renal defect, JS with oculorenal defects, JS with hepatic defect and JS with orofaciodigital defects.[1] To date, 17 causative genes have been identified in JSRD: *INPP5E*,[2] *TMEM216*,[3] *AHI1*,[4] *NPHP1*,[5] *CEP290*,[6] *TMEM67*,[7] *RPGRIP1L*,[8] *ARL13B*,[9] *CC2D2A*,[10] *OFD1*,[11] *TTC21B*,[12] *KIF7*,[13] *TCTN1*,[14] *TMEM237*,[15] *CEP41*,[16] *TMEM138*,[17] and *C5ORF42*.[18] Because of the clinical and genetic heterogeneity in JSRD, it can be very difficult to identify the causative mutations in individual cases.

We encountered five non-consanguineous Japanese families with JSRD (Figure 1a) and molar tooth sign was observed in all patients (Figures 1b–e, Supplementary Table 1). Peripheral blood samples were obtained from patients and their family members after written informed consent was given. To identify causative mutations, we performed whole-exome sequencing (WES) in five probands of the five families (one proband from each family). DNA was processed using the SureSelectXT Human All Exon 50 Mb library or V4 (51 Mb) library (Agilent Technologies, Santa Clara, CA, USA), and sequenced on a Genome Analyzer IIx sequencer (Illumina, San Diego, CA, USA) with 108 bp paired-end reads, or on a HiSeq2000 sequencer (Illumina) with 101 bp paired-end reads and 7 bp index reads. Image analysis and base calling were performed by Illumina pipeline. Approximately 3.8–6.0 Gb of sequence data were mapped to the human reference genome (GRCh37.1/hg19) with Novoalign or Burrows-Wheeler Aligner. The mean depth of coverage was 55–125 reads, with 88–96% of all coding exons being covered by 5 × or more reads.

Out of all variants within exons and ± 20-bp intronic regions from the exon–intron boundaries, those registered in dbSNP135, 1000 Genomes and ESP5400 and located within the segmental duplications were removed. Homozygous or compound heterozygous variants of 17 JSRD causative genes were then picked up. In patients 1, 2, 3 and 4 whose DNA was captured by the SureSelectXT Human All Exon 50 Mb library, ~90% of the entire coding regions in 13 of 17 causative genes were covered by 5 × reads or more. In patient 5 captured by the V4 (51 Mb) library, >90% of the coding region was covered by 5 × reads or more (Supplementary Table 2), indicating that the V4 library offered superior coverage to the SureSelectXT library around the regions of the JSRD genes.

All patients from the five families possessed novel compound heterozygous mutations or a homozygous mutation in known genes later confirmed by Sanger sequencing (Figure 1a): c.1862G>A (p.R621Q)/c.700dupC (p.L234Pfs*56) in *INPP5E* (9q34.3) for family 1; c.5788A>T (p.K1930*)/c.6012-12A>T in *CEP290* (12q21.32) for family 2; c.329A>G (p.D110G)/c.2322 + 5delG in *TMEM67* (8q22.1) for family 3; homozygous c.6012-12A>T in *CEP290* for family 4; and c.214G>T (p.E72*)/c.6012-12A>T in *CEP290* for family 5. No other variants within 17 known genes have been identified after excluding

[1]Department of Human Genetics, Yokohama City University Graduate School of Medicine, Yokohama, Japan; [2]Department of Pediatrics, Gunma University Graduate School of Medicine, Maebashi, Japan; [3]Department of Nephrology, Chiba Children's Hospital, Chiba, Japan and [4]National Center for Child Health and Development, Tokyo, Japan
Correspondence: Dr N Miyake, Department of Human Genetics, Yokohama City University Graduate School of Medicine, 3-9 Fukuura, Kanazawa-ku, Yokohama 236-0004, Japan.
E-mail: nmiyake@yokohama-cu.ac.jp
Received 31 July 2012; revised 3 September 2012; accepted 5 September 2012

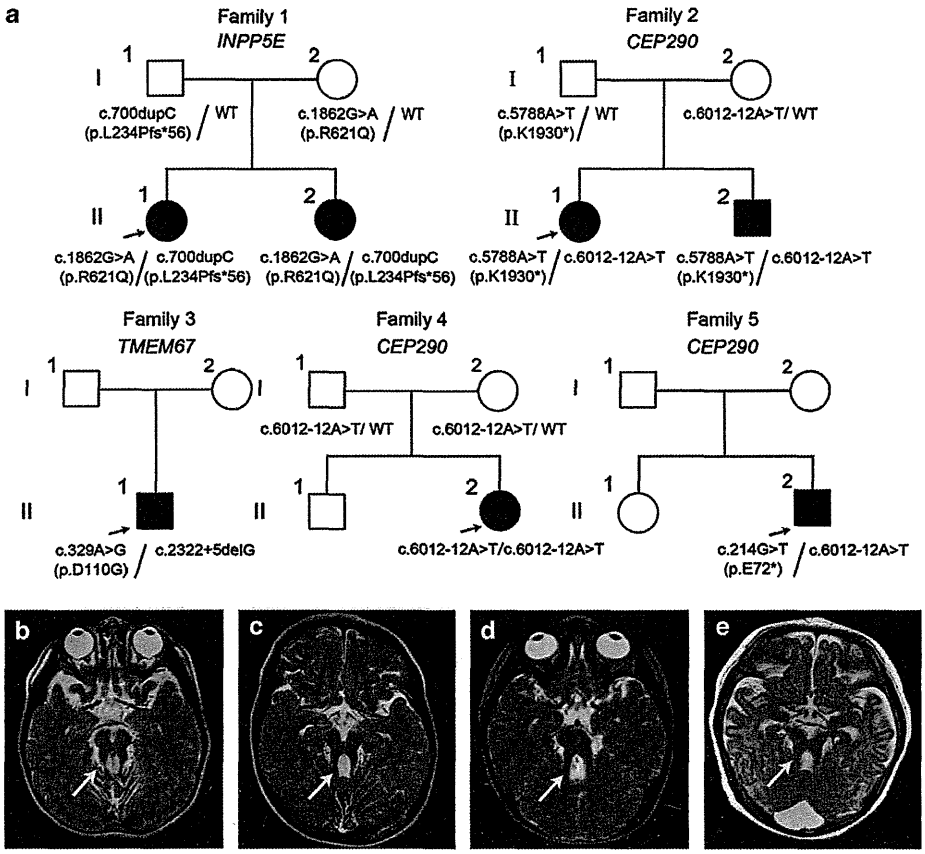

Figure 1 Familial pedigree and brain MRI of the patients. (**a**) JSRD families and mutations. (**b**) T2-weighted axial images of III-1, family 1. (**c**) T2-weighted axial images of III-2, family 1. (**d**) T2-weighted axial images of III-1, family 2. (**e**) T2-weighted axial images of III-2, family 2. The molar tooth sign is visible in all patients (arrowheads).

the variants of dbSNP135, 1000 Genomes and ESP5400. Clinical phenotypes caused by respective mutated genes are discussed in Supplementary text. In families 1, 2 and 4 in which parental samples were available, all parents were heterozygous carriers of one of the mutations. As parental samples were unavailable from families 3 and 5, we determined whether two mutations resided on different alleles by cloning an reverse transcriptase-PCR (RT-PCR) product amplified from total RNA of lymphoblastoid cells into a pCR4-TOPO vector (Life Technologies, Carlsbad, CA, USA) and sequencing. Each mutation was found in a different allele for both families (data not shown). Another variant, c.1894A>G (p.K632E) in *CEP290*, of family 2 was not found to be pathogenic based on web-based analyses such as SIFT, PolyPhen-2 and Mutation Taster (Supplementary Table 3). In families 2, 4 and 5 with a *CEP290* abnormality, c.6012-12A>T was shared. On the basis of our in-house 135 exome data, the allele frequency of the mutation was 1/270 allele (0.74%), indicating that it may be a rare variant in Japanese. The other mutations were not found in our in-house 135 exome data.

Splicing effects were examined in families 3 and 4. RT-PCR was performed on RNA from lymphoblastoid cells of family members using primers spanning exons 42/43 and 45/46 in family 4 and exons 20/21 and 24/25 in family 3 (sequence information available on request). In family 4, only an aberrant cDNA was detected in II-2, whereas the parents (I-1 and I-2) showed two different products including one wild-type, which was detected in a control (Supplementary Figures 1a, b). Sequencing of the mutant product revealed a 57-bp insertion corresponding to the 3′-side of intron 43. As a result, a premature stop codon was introduced at intron 43. In family 3, RT-PCR detected a mutant cDNA in II-1 together with a wild-type product, which was detected in a control. Sequencing of the mutant product confirmed the skipping of exon 22, resulting in an in-frame 27 amino-acid deletion (Supplementary Figures 1c, d).

WES has proved a powerful tool for the identification of novel genes in genetic diseases. It also has tremendous potential for clinical diagnosis and is now being applied in the molecular diagnosis of single-gene disorders such as neurofibromatosis type 1, Marfan syndrome and multi-gene disorders such as retinitis pigmentosa.[19] As shown here, WES would also be suitable for the diagnosis of JSRD, another multi-gene disorder. Though the read-coverage of the old version of SureSelect did not sufficiently collect genomic DNAs for four genes (*INPP5E*, *TMEM216*, *KIF7* and *TCTN1*), the performance of the V4 (51 Mb) library was satisfactory for all genes. Further, as exome capture technology is based on hybridization it can be refractory to homologous regions, so other methods such as multiplex PCR amplification and multiple microdroplet PCR technology could be useful in addition.

In conclusion, we were able to identify causative mutations in five non-consanguineous families with JSRD using WES. The diagnostic utility of WES is obvious, implying that WES or other next-generation sequencing technologies will be a main factor of molecular diagnosis.

ACKNOWLEDGEMENTS

We thank the patients and their families for their participation in this study. This work was supported by research grants from the Ministry of Health, Labor and Welfare (HS, N Matsumoto, N Miyake), the Japan Science and Technology Agency (N Matsumoto), the Strategic Research Program for Brain Sciences (N Matsumoto) and a Grant-in-Aid for Scientific Research on Innovative Areas-(Transcription cycle)-from the Ministry of Education, Culture, Sports, Science and Technology of Japan (N Matsumoto), a Grant-in-Aid for Scientific Research from Japan Society for the Promotion of Science (N Matsumoto), a Grant-in-Aid for Young Scientist from Japan Society for the Promotion of Science (HS, N Miyake) and a grant from the Takeda Science Foundation (N Matsumoto, N Miyake).

Web Resources: The URLs for data presented herein are as follows: Novoalign, http://www.novocraft.com/main/index.php: Burrows-Wheeler Aligner, http://bio-bwa.sourceforge.net/: SIFT, http://sift.jcvi.org/: PolyPhen-2, http://genetics.bwh.harvard.edu/pph2/: Mutation Taster, http://neurocore.charite.de/MutationTaster/

1 Brancati, F., Dallapiccola, B. & Valente, E. M. Joubert Syndrome and related disorders. *Orphanet. J. Rare Dis.* **5,** 20 (2010).
2 Bielas, S. L., Silhavy, J. L., Brancati, F., Kisseleva, M. V., Al-Gazali, L., Sztriha, L. *et al.* Mutations in INPP5E, encoding inositol polyphosphate-5-phosphatase E, link phosphatidyl inositol signaling to the ciliopathies. *Nat. Genet.* **41,** 1032–1036 (2009).
3 Valente, E. M., Logan, C. V., Mougou-Zerelli, S., Lee, J. H., Silhavy, J. L., Brancati, F. *et al.* Mutations in TMEM216 perturb ciliogenesis and cause Joubert, Meckel and related syndromes. *Nat. Genet.* **42,** 619–625 (2010).
4 Ferland, R. J., Eyaid, W., Collura, R. V., Tully, L. D., Hill, R. S., Al-Nouri, D. *et al.* Abnormal cerebellar development and axonal decussation due to mutations in AHI1 in Joubert syndrome. *Nat. Genet.* **36,** 1008–1013 (2004).
5 Parisi, M. A., Bennett, C. L., Eckert, M. L., Dobyns, W. B., Gleeson, J. G., Shaw, D. W. *et al.* The NPHP1 gene deletion associated with juvenile nephronophthisis is present in a subset of individuals with Joubert syndrome. *Am. J. Hum. Genet.* **75,** 82–91 (2004).
6 Valente, E. M., Silhavy, J. L., Brancati, F., Barrano, G., Krishnaswami, S. R., Castori, M. *et al.* Mutations in CEP290, which encodes a centrosomal protein, cause pleiotropic forms of Joubert syndrome. *Nat. Genet.* **38,** 623–625 (2006).
7 Baala, L., Romano, S., Khaddour, R., Saunier, S., Smith, U. M., Audollent, S. *et al.* The Meckel-Gruber syndrome gene, MKS3, is mutated in Joubert syndrome. *Am. J. Hum. Genet.* **80,** 186–194 (2007).
8 Arts, H. H., Doherty, D., van Beersum, S. E., Parisi, M. A., Letteboer, S. J., Gorden, N. T. *et al.* Mutations in the gene encoding the basal body protein RPGRIP1L, a nephrocystin-4 interactor, cause Joubert syndrome. *Nat. Genet.* **39,** 882–888 (2007).
9 Cantagrel, V., Silhavy, J. L., Bielas, S. L., Swistun, D., Marsh, S. E., Bertrand, J. Y. *et al.* Mutations in the cilia gene ARL13B lead to the classical form of Joubert syndrome. *Am. J. Hum. Genet.* **83,** 170–179 (2008).
10 Gorden, N. T., Arts, H. H., Parisi, M. A., Coene, K. L., Letteboer, S. J., van Beersum, S. E. *et al.* CC2D2A is mutated in Joubert syndrome and interacts with the ciliopathy-associated basal body protein CEP290. *Am. J. Hum. Genet.* **83,** 559–571 (2008).
11 Coene, K. L., Roepman, R., Doherty, D., Afroze, B., Kroes, H. Y., Letteboer, S. J. *et al.* OFD1 is mutated in X-linked Joubert syndrome and interacts with LCA5-encoded lebercilin. *Am. J. Hum. Genet.* **85,** 465–481 (2009).
12 Davis, E. E., Zhang, Q., Liu, Q., Diplas, B. H., Davey, L. M., Hartley, J. *et al.* TTC21B contributes both causal and modifying alleles across the ciliopathy spectrum. *Nat. Genet.* **43,** 189–196 (2011).
13 Dafinger, C., Liebau, M. C., Elsayed, S. M., Hellenbroich, Y., Boltshauser, E., Korenke, G. C. *et al.* Mutations in KIF7 link Joubert syndrome with Sonic Hedgehog signaling and microtubule dynamics. *J. Clin. Invest.* **121,** 2662–2667 (2011).
14 Garcia-Gonzalo, F. R., Corbit, K. C., Sirerol-Piquer, M. S., Ramaswami, G., Otto, E. A., Noriega, T. R. *et al.* A transition zone complex regulates mammalian ciliogenesis and ciliary membrane composition. *Nat. Genet.* **43,** 776–784 (2011).
15 Huang, L., Szymanska, K., Jensen, V. L., Janecke, A. R., Innes, A. M., Davis, E. E. *et al.* TMEM237 is mutated in individuals with a Joubert syndrome related disorder and expands the role of the TMEM family at the ciliary transition zone. *Am. J. Hum. Genet.* **89,** 713–730 (2011).
16 Lee, J. E., Silhavy, J. L., Zaki, M. S., Schroth, J., Bielas, S. L., Marsh, S. E. *et al.* CEP41 is mutated in Joubert syndrome and is required for tubulin glutamylation at the cilium. *Nat. Genet.* **44,** 193–199 (2012).
17 Lee, J. H., Silhavy, J. L., Lee, J. E., Al-Gazali, L., Thomas, S., Davis, E. E. *et al.* Evolutionarily assembled cis-regulatory module at a human ciliopathy locus. *Science* **335,** 966–969 (2012).
18 Srour, M., Schwartzentruber, J., Hamdan, F. F., Ospina, L. H., Patry, L., Labuda, D. *et al.* Mutations in C5ORF42 Cause Joubert Syndrome in the French Canadian Population. *Am. J. Hum. Genet.* **90,** 693–700 (2012).
19 Zhang, W., Cui, H. & Wong, L. J. Application of next generation sequencing to molecular diagnosis of inherited diseases. *Top. Curr. Chem.* (e-pub ahead of print 11 May 2012; doi:10.1007/128_2012_325).

Supplementary Information accompanies the paper on Journal of Human Genetics website (http://www.nature.com/jhg)

ELSEVIER

Brain & Development xxx (2012) xxx–xxx

BRAIN & DEVELOPMENT
Official Journal of the Japanese Society of Child Neurology

www.elsevier.com/locate/braindev

Original article

Neuropathology of leukoencephalopathy with brainstem and spinal cord involvement and high lactate caused by a homozygous mutation of DARS2

Sumimasa Yamashita [a,*], Noriko Miyake [b], Naomichi Matsumoto [b], Hitoshi Osaka [a], Mizue Iai [a], Noriko Aida [c], Yukichi Tanaka [d]

[a] *Division of Child Neurology, Kanagawa Children's Medical Center, Japan*
[b] *Department of Human Genetics, Yokohama City University Graduate School of Medicine, Japan*
[c] *Division of Radiology, Kanagawa Children's Medical Center, Japan*
[d] *Division of Pathology, Kanagawa Children's Medical Center, Japan*

Received 23 November 2011; received in revised form 7 April 2012; accepted 9 May 2012

Abstract

We diagnosed three siblings from consanguineous east Asian parents with leukoencephalopathy with brainstem and spinal cord involvement and high lactate (LBSL) from characteristic MRI, MRS findings and a homozygous mutation in the DARS2 gene. The neurological symptoms of the three patients consisted of psychomotor developmental delay, cerebellar ataxia since infancy, spasticity in the initial phase and peripheral neuropathy in later stages. Their mental development was delayed, but did not deteriorate. MRI signal abnormalities included the same abnormalities reported previously but tended to be more extensive. Signal abnormalities in the cerebral and cerebellar white matter were homogeneous and confluent from early stages. In addition, other tract such as the central tegmental tract was involved. Furthermore, an atrophic change in the cerebral white matter was observed on follow-up in one case. Two of the patients were autopsied and neuropathological findings revealed characteristic vacuolar changes in the white matter of the cerebrum, cerebellum and the nerve tracts of the brain stem and spinal cord. The central myelin sheath showed intralamellar splitting by electron microscopy. These findings were consistent to a spongy degeneration in the diffuse white matter of the brain, or spongiform leukoencephalopathy. In addition, peripheral nerves showed both axonal degeneration and abnormal myelin structures. We discussed the relationship between deficits in mitochondrial aspartyl-tRNA synthetase activity and the neuropathology observed.

Keywords: LBSL; DARS2; MRS; Cerebellar ataxia; Spongy encephalopathy; Axonal degeneration

1. Introduction

Recently, the clinical features and magnetic resonance image (MRI) characteristics of leukoencephalopathy with brainstem and spinal cord involvement and lactate elevation (LBSL) have been described [1]. MRI and ^{1}H-Magnetic resonance spectroscopy (MRS) of LBSL patients show significant signal abnormalities in the brainstem and spinal cord, as well as cerebral white matter. LBSL is caused by mutations of the *DARS2* gene encoding mitochondrial aspartyl-tRNA synthetase (MtAspRS) [2]. *DARS2* mutations have been found in all reported patients [2–7], but all have been compound heterozygotes. In this report, we examine a consanguineous family with three individuals affected with LBSL

* Corresponding author. Address: Division of Child Neurology, Kanagawa Children's Medical Center, Mutsukawa 2-138-4 Minami-ku, Yokohama, Kanagawa 232-8555, Japan. Tel.: +81 45 711 2351; fax: +81 45 721 3324.
E-mail address: syamashita@kcmc.jp (S. Yamashita).

0387-7604/$ - see front matter © 2012 The Japanese Society of Child Neurology. Published by Elsevier B.V. All rights reserved.
http://dx.doi.org/10.1016/j.braindev.2012.05.007

Please cite this article in press as: Yamashita S et al. Neuropathology of leukoencephalopathy with brainstem and spinal cord involvement and high lactate caused by a homozygous mutation of DARS2.. Brain Dev (2012), http://dx.doi.org/10.1016/j.braindev.2012.05.007

caused by a homozygous *DARS2* mutation [8], which may explain more severe symptoms than compound heterozygous [9]. Neuropathological examination including autopsies of two of the cases revealed confirmed LBSL. This is the first autopsy report of the patients with LBSL.

2. Case report

Three of four siblings were affected by the same disorder. Their parents were consanguineous cousins. In this family, the great-grand father was of Chinese origin and the great-grand mother was Japanese. There were no other family members with the same disorder. The eldest sister, aged 24 years, is healthy, and Case 1 is the second sister affected, but is alive. Cases 2 and 3 were the third and forth siblings. Both were affected and died of the disorder.

Case 1: 23 year old female. Case 1 had no eventful neonatal history. She could walk and speak several words at 1 year old. She suffered from ataxic gait at 3 years, and was admitted to our hospital at 5 years. On examination, hypotonia, horizontal nystagmus, dysdiadochokinesis, intention tremor of upper extremities, and slurred speech were observed. Deep tendon reflexes (DTRs) in her upper and lower extremities were elicited normally. DTRs disappeared completely at the age of 7 years in her lower extremities and at 13 years in her upper extremities. She lost the ability to walk with support at 7 years, and required a wheel chair. Her mental development was delayed severely. At the current age of 23 years, she is wheel-chair bound, but driving approximately 10 m by herself.

Case 2: 8 year old female at autopsy, younger sister of Case 1. Case 2 was able to sit alone at the age of 6 months, but she did not obtain any motor development. She showed ataxia, mild muscle hypertonia, hyperreflexia in Achilles tendon reflex, positive Babinski reflex, positive foot clonus, intention tremor, nystagmus, slurred speech, and mental retardation at 5 years old. Her muscle tonus turned to hypotonus at 8 years. She died from respiratory distress and pneumonia at 8 years.

Case 3: 2 year old male at autopsy, younger brother of Case 1. Case 3 could sit alone at the age of 5 months and walk with support at the age of 1 year and 4 months. He could speak several words at that time, although he showed ataxia. At age 2, his muscle tonus was increased

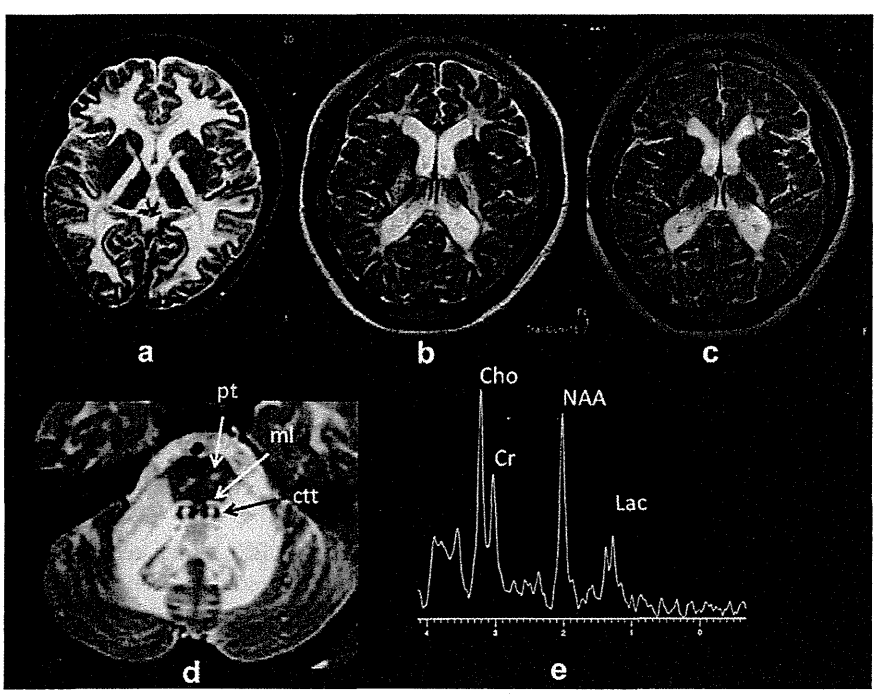

Fig. 1. MRI and MR spectroscopy of Case 1. (a) T2-WI of the cerebrum at 10 years old. (b) T2-WI of the cerebrum at 18 years old. (c) T2-WI of the cerebrum at 22 years old. (d) T2-WI. Pons and cerebellum at 10 years old. pt, pyramidal tract; ml, medial lemniscus; ctt, central tegmental tract. (e) MR spectroscopy of the cerebral white matter at 10 years old. Cho, choline; Cr, creatine; NAA, N-acetyl aspartic acid; Lac, lactate (PRESS sequence, TR/TE = 2000/270). There was homogeneous diffuse prolongation of T1 and T2 signals in the entire cerebral white matter that extended from immediately below the cortex to the deep white matter in all three cases [8]. As a result, U-fibers were spared well in the frontal lobe, moderately in parietal and temporal lobe, but were not preserved in the occipital lobe. The same strong signal abnormalities as the cerebral white matter were seen in the posterior limb of the internal capsule in all cases. Progressive atrophic change in cerebral white matter including the posterior limb of the internal capsule developed gradually, which MRI demonstrated at the age of 10, 18 and 22 years (a–c). Marked involvement of the diffuse white matter of the cerebellum and of the central tegmental tracts was observed (d). MR spectroscopy showed high lactate level at the age of 10 years (e).

Please cite this article in press as: Yamashita S et al. Neuropathology of leukoencephalopathy with brainstem and spinal cord involvement and high lactate caused by a homozygous mutation of DARS2.. Brain Dev (2012), http://dx.doi.org/10.1016/j.braindev.2012.05.007

and he had hyperreflexia, positive Babinski reflex, and horizontal nystagmus, but no tremor in his fingers. He expired from respiratory failure after febrile illness at age 2.

A detailed biochemical examination was performed in all three patients, but revealed no definite abnormalities. Serum lactate levels in each patient were within normal limits, although cerebrospinal fluid (CSF) lactate was no more than a borderline elevation. In Case 1, CSF lactate was 24.3 mg/dl (normal range <ca.23). In each case, motor nerve conduction velocity (MCV) was within the normal range in infancy, but decreased gradually, and the amplitudes of compound muscle action potential was decreased since the infantile ages. In Case 1, MCV showed 50 m/sec at the median nerve at the age of 10. EMG showed a neurogenic pattern in the upper extremity and fibrillation in the lower extremity. In Case 3, MCV showed 42.3 m/sec in the median nerve at the age of 2 years.

The MRI findings of the three cases (Fig. 1) revealed similar features and meet the criteria of LBSL described by the previous report [1]. The findings of our cases, however, were characterized by the following four points. First, similar strenuous and diffuse cerebral white matter involvement was observed in all three cases. Second, progressive atrophic change in cerebral white matter developed gradually, which MRI demonstrated at the age of 10, 18 and 22 years in Case 1 (Fig. 1a–c). Third, marked diffuse involvement of the white matter of the cerebellum was observed (Fig. 1d). Fourth, marked involvement of the central tegmental tracts was observed (Fig. 1d).

By MR spectroscopy, high lactate levels were observed in Cases 1 (Fig. 1e) and 3. Reexamination of Case 1 at age 22 years revealed a slight elevation of lactate, but it was lower than that at 10 years.

Direct sequencing of *DARS2* gene revealed a homozygous c.228-22T>A in the three affected and heterozygous c.228-22T>A in the parents and healthy sister. This intronic mutation change led to the skipping of exon 3, low transcription, and faint protein level in proband fibroblasts [8]. Therefore, a diagnosis of LBSL was obtained in our cases.

3. Neuropathology

We re-evaluated the autopsy finding of Cases 2 and 3 retrospectively and clarified the disease mechanism after obtaining the result of genetic analysis. In both patients, neuropathological findings were similar in the central nervous system. Vacuolar changes in the cerebral white matter began immediately below the cortex (Fig. 2a). Deeper, the more spongy alterations were observed as a large number of vacuoles and astrocytes in the white matter (Fig. 2b). The neuropil was rarefacted, and many macrophages had infiltrated into the deep white matter. As a result, demyelination and axonal degeneration was observed in the deeper white matter. The central myelin sheath showed intralamellar splitting of the outermost

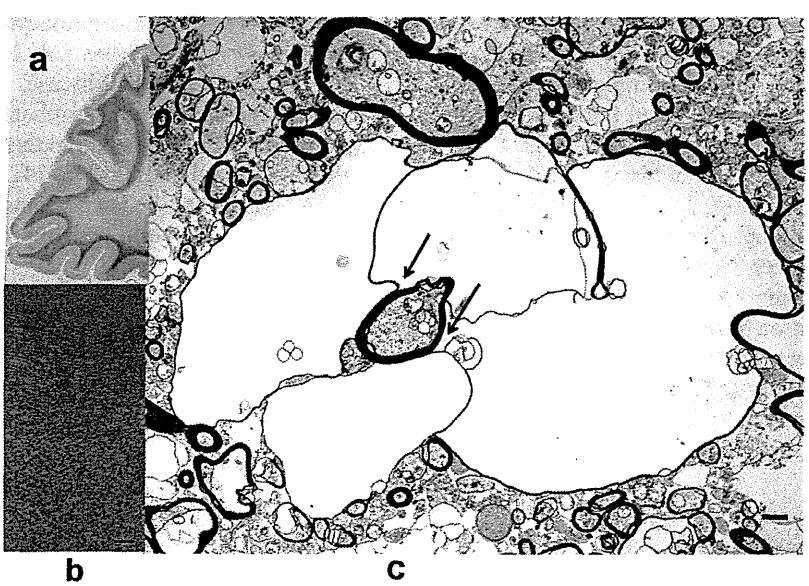

Fig. 2. Neuropathological findings of the cerebrum. (a) Frontal lobe of the cerebrum of Case 2. KB stain. Myelin pallor is diffuse in the cerebral white matter. (b) Microscopic finding of frontal lobe of the cerebrum of Case 2. KB stain. Vacuolar changes in the cerebral white matter began immediately below the cortex (top). The subcortical U-fibers were spared in the frontal lobe and myelinated fibers were preserved. The deeper (bottom) regions show more spongy alterations. A large number of vacuoles and astrocytes exist in the white matter. Scale 100 μm. (c) Electron microscopic findings of the cerebrum of Case 3. The central myelin sheath shows intralamellar splitting (←) of the outermost myelin lamellae. Scale 1 μm.

Please cite this article in press as: Yamashita S et al. Neuropathology of leukoencephalopathy with brainstem and spinal cord involvement and high lactate caused by a homozygous mutation of DARS2.. Brain Dev (2012), http://dx.doi.org/10.1016/j.braindev.2012.05.007

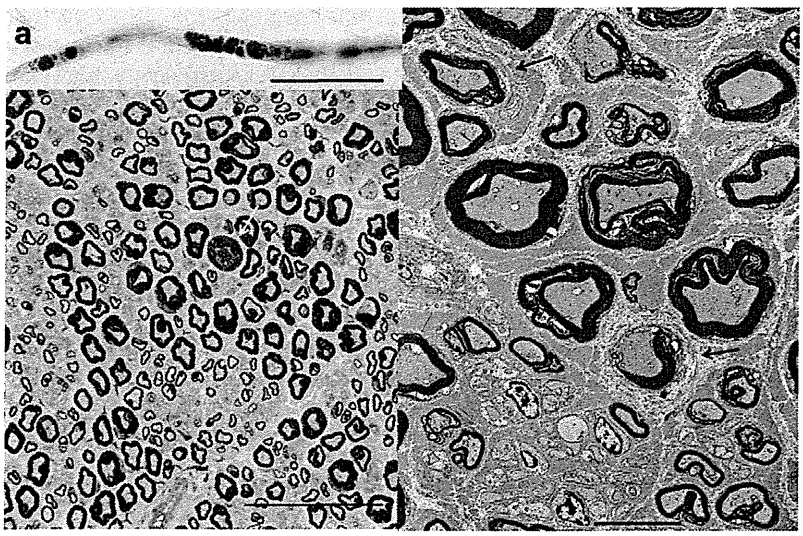

Fig. 3. Neuropathological findings of the autopsied sural nerve of Case 3. (a) Microscopy of the sural nerve by teased fiber examination. Typical formation of many myelin ovoids along a myelinated fiber is observed. Scale 100 μm. (b) Epon-embedded semi-thin section with toluidine blue staining. The numbers of myelinated nerve fibers is reduced mildly or moderately with an extracellular endoneurial connective tissue expansion. Abnormal myelin layer folding, myelin separation at the inside of layers, partial myelin clusters of various sizes associated with myelin separation and partial thin myelin layers were characteristic. Axonal degeneration (⇦) within several myelinated fibers is observed. Scale 50 μm. (c) Electron microscopic findings of the sural nerve. Abnormal myelin layer folding, myelin separation at the inside of layers, partial myelin clusters of various sizes and partial thin myelin layers are observed. Onion bulb formation (←) is seen surrounding a few myelinated fibers by poor Schwann cell cytoplasm, but atypical onion bulb was recognized frequently in several layers of basal lamina, and abnormal Schwann cell processes around unmyelinated fibers were observed. No abnormal crystalline structure was observed in the mitochondria. Scale 10 μm.

myelin lamellae by electron microscopic examination (Fig. 2c). The cerebral cortical layers showed normal structures and no abnormal storage materials in the neuronal cells. Purkinje cells of the cerebellum were lost moderately and Bergmann's glial cells were increased. Cerebellar white matter showed similar alteration as the cerebrum. The neuropathological findings indicated spongy degeneration of the white matter.

The sural nerve was investigated in three cases. In the teased fiber examination (Fig. 3a), typical formation of many myelin ovoids along a few myelinated fibers was observed in all three cases. Neither segmental demyelination nor remyelination was a predominant feature. Microscopic examination revealed that the numbers of myelinated nerve fibers was reduced mildly or moderately (Fig. 3b). Axonal degeneration within several myelinated fibers was observed in Cases 1 and 3.

4. Discussion

The pathologically characteristic findings revealed a spongy degeneration in the diffuse white matter of the brain. This pathological finding is apparent in many inherited metabolic and degenerative neurological disorders [10–12]. Intralamellar split of the myelin sheaths contributed to forming variable vacuoles in the white matter. In addition, a noteworthy finding was axonal degeneration of the peripheral nerves in our patients. This finding is an important feature of LBSL as described by Isohanni et al. [4]. Mutations in the genes encoding cytoplasmic aminoacyl-tRNA synthetases for glycine [13] and tyrosine [14] have been identified in Charcot–Marie–Tooth disease. Both disorders show axonal degeneration of peripheral nerves because these synthetases localize to axonal termini and have a specific role in neuronal endings [13–14]. In our cases, aspartyl-tRNA synthetase deficiency has proved to induce an axonal type peripheral neuropathy.

Conflicts of interest

The authors have no conflict of interest to declare.

References

[1] Van der Knaap MS, van der Voorn P, Barkhof F, van Costr R, Klägeloh-Mann I, Feigenbaum A, et al. A new leukodystrophy with brainstem and spinal cord involvement and high lactate. Ann Neurol 2003;53:252–8.

[2] Scheper GC, van der Klok T, van Andel R, van Berkel CGM, Sissler M, Smet J, et al. Mitochondrial aspartyl-tRNA synthetase deficiency causes leukoencephalopathy with brain stem and spinal cord involvement and lactate elevation. Nat Genet 2007;39:534–9.

[3] Uluc K, Baskan O, Yildirim KA, Ozsahin S, Koseoglu M, Isak B, et al. Leukoencepahalopathy with brain stem and spinal cord involvement and high lactate: a genetically proven case with distinct MRI findings. J Neurol Sci 2008;273:118–22.

Please cite this article in press as: Yamashita S et al. Neuropathology of leukoencephalopathy with brainstem and spinal cord involvement and high lactate caused by a homozygous mutation of DARS2.. Brain Dev (2012), http://dx.doi.org/10.1016/j.braindev.2012.05.007